12

THE CALIBRATION AND APPLICATION OF FIVE-HOLE PROBES

A. L. Treaster, A. M. Yocum.

TM-78-10

Technical Memorandum
File No. TM 78-10
January 18, 1978
Contract No. N00017-73-C-1418, NSG-3031
Copy No. 26

18 Jan 78

54 P.

The Pennsylvania State University
Institute for Science and Engineering
APPLIED RESEARCH LABORATORY
Post Office Box 30
State College, Pa. 16801

NAVY DEPARTMENT

NAVAL SEA SYSTEMS COMMAND

UNCLASSIFIED

SECURITY CLASSIFICATION OF THIS PAGE *(When Data Entered)*

REPORT DOCUMENTATION PAGE		READ INSTRUCTIONS BEFORE COMPLETING FORM
1. REPORT NUMBER TM 78-10	2. GOVT ACCESSION NO.	3. RECIPIENT'S CATALOG NUMBER
4. TITLE *(and Subtitle)* THE CALIBRATION AND APPLICATION OF FIVE-HOLE PROBES (U)		5. TYPE OF REPORT & PERIOD COVERED Technical Memorandum 6. PERFORMING ORG. REPORT NUMBER
7. AUTHOR(s) A. L. Treaster and A. M. Yocum		8. CONTRACT OR GRANT NUMBER(s) N00017-73-C-1418
9. PERFORMING ORGANIZATION NAME AND ADDRESS Applied Research Laboratory P. O. Box 30 State College, PA 16801		10. PROGRAM ELEMENT, PROJECT, TASK AREA & WORK UNIT NUMBERS
11. CONTROLLING OFFICE NAME AND ADDRESS Naval Sea Systems Command Washington, DC 20362		12. REPORT DATE January 18, 1978 13. NUMBER OF PAGES 51
14. MONITORING AGENCY NAME & ADDRESS*(if different from Controlling Office)*		15. SECURITY CLASS. *(of this report)* UNCLASSIFIED 15a. DECLASSIFICATION/DOWNGRADING SCHEDULE

16. DISTRIBUTION STATEMENT *(of this Report)*

Approved for Public Release. Distribution Unlimited.
Per NAVSEA - January 31, 1978

17. DISTRIBUTION STATEMENT *(of the abstract entered in Block 20, if different from Report)*

18. SUPPLEMENTARY NOTES

Presented at 24th International Symposium, Albuquerque, New Mexico

19. KEY WORDS *(Continue on reverse side if necessary and identify by block number)*

five-hole probe
flow measurement
calibration

20. ABSTRACT *(Continue on reverse side if necessary and identify by block number)*

(U) In many complex flow fields such as those encountered in turbomachines, the experimental determination of the steady-state, three-dimensional characteristics of the flow field are frequently required. If space limitations or other considerations make nulling techniques impractical, five-hole probes in a non-nulling mode can be employed. However, this application requires complete three-dimensional calibration data which → next page

DD FORM 1 JAN 73 1473 EDITION OF 1 NOV 65 IS OBSOLETE UNCLASSIFIED

SECURITY CLASSIFICATION OF THIS PAGE *(When Data Entered)*

are not usually supplied by commercial vendors. Presented in this paper are the results of programs to calibrate and employ five-hole probes of both angle-tube and prismatic geometries. Included are descriptions of the calibration technique, typical calibration data, and an accompanying discussion of the application or interpolation procedure. Also documented are the variations in the calibration data due to Reynolds number and wall proximity effects. Typical measured data are included and, where applicable, these data are validated by comparison with data obtained using other types of velocity measuring instrumentation.

Subject: The Calibration and Application of Five-Hole Probes

References: See page 27.

Abstract: In many complex flow fields such as those encountered in turbomachines, the experimental determination of the steady-state, three-dimensional characteristics of the flow field are frequently required. If space limitations or other considerations make nulling techniques impractical, five-hole probes in a non-nulling mode can be employed. However, this application requires complete three-dimensional calibration data which are not usually supplied by commercial vendors. Presented in this paper are the results of programs to calibrate and employ five-hole probes of both angle-tube and prismatic geometries. Included are descriptions of the calibration technique, typical calibration data, and an accompanying discussion of the application or interpolation procedure. Also documented are the variations in the calibration data due to Reynolds number and wall proximity effects. Typical measured data are included and, where applicable, these data are validated by comparison with data obtained using other types of velocity measuring instrumentation.

Acknowledgment: This paper has been prepared for presentation at the 24th International Instrumentation Symposium sponsored by the Instrumentation Society of America (ISA).

The work was sponsored by NAVSEA Code 03, and NASA Grant NSG 3031.

Table of Contents

List of Figures

Nomenclature

$C_{P_{pitch}}$	pitch coefficient defined by Equation (2)
$C_{P_{static}}$	static pressure coefficient defined by Equation (4)
$C_{P_{total}}$	total pressure coefficient defined by Equation (3)
$C_{P_{yaw}}$	yaw coefficient defined by Equation (1)
d	characteristic probe diameter, ft
$\overline{P}$	an average pressure defined by Equation (5), psfa
P_1	pressure measured at the central probe hole (Figures (1) and (2)), psfa
P_2 and P_3	pressures measured in the yaw plane (Figures (1) and (2)), psfa
P_4 and P_5	pressures measured in the pitch plane (Figures (1) and (2)), psfa
P_i	any numbered pressure, psfa
P_{ref}	a reference pressure, psfa
P_{static}	the true, local static pressure at the sensing element, psfa
P_{total}	the true, local total pressure at the sensing element, psfa
R_d	$(V_\infty \cdot d)/\nu$ = Reynolds number
$\overline{V}$	the magnitude of the velocity vector at the probe sensing element, fps
V_∞	reference or free stream velocity, fps
V_R, V_X, V_θ	the three orthogonal velocity components defined in Figures (1) and (2), fps
α	angle in the pitch plane, degrees
β	angle in the yaw plane, degrees
Δ	indicates a pressure difference, psfa
ρ	fluid mass density, slugs/ft^3
ν	kinematic viscosity, ft^2/sec

INTRODUCTION

In many complex flow fields such as those encountered in turbomachines, the experimental determination of the steady-state, three-dimensional characteristics of the flow field are required. If space limitations, or other considerations, make nulling techniques impractical, five-hole probes in a non-nulling mode can be employed for measurements in low speed, incompressible flows. This application requires three-dimensional calibration data which are not usually supplied by commercial vendors. Thus, the measurement of these data and the development of an interpolation procedure to employ these calibration data become the responsibility of the user.

The application of five-hole probes is not new but dates back as far as Admiral Taylor's work in 1915, Reference [1]. Other work followed; but Pien, Reference [2], was the first to show theoretically that for a spherical probe the velocity component in any plane in space can be obtained independently from three pressure measurements in that plane. Although this potential flow solution is valid for perfectly formed spherical probes in inviscid flows of restricted angularity, Pien found it necessary to obtain experimental calibration data. The initial program employing five-hole probes at the Applied Research Laboratory of The Pennsylvania State University involved the measurement of the three-dimensional wake in the propeller plane of a surface ship model installed in the test section of the 48-inch diameter Garfield Thomas Water Tunnel, References [3] and [4]. Since the probes employed in this study were of angle-tube and prismatic geometries, the approach of Krause and Dudzinski, Reference [5], which includes geometric and viscous effects was most applicable. However, this method required extension to enable the measurement of

the local pressures and the magnitude and direction of the corresponding velocity at the probe tip.

Because the goals of the ARL/PSU five-hole probe program were application oriented, the objectives of the five-hole probe phase of the program were rather pragmatic in nature. Primary objectives were specified in three areas: (1) calibration: to develop the necessary hardware and experimental procedures to use existing test facilities for the calibration of the five-hole probes; (2) analysis: to develop interpolation and data reduction procedures which use the calibration data and the measured pressures to define the velocity vector at the probe tip; and (3) measurement: to survey known and unknown three-dimensional flow fields.

Discussed in the following pages are the probe design considerations, the calibration device, the calibration procedure, the comparison of calibration data for different geometries, and the data analysis techniques employed in the development of the five-hole probe system. Because calibration data should be independent of measured quantities, the effects of Reynolds number variations were assessed by calibrating the prism probes in air over Reynolds number range of 2000 to 7000. The angle-tube probes were calibrated in water at a Reynolds number of 20,000 and in air at 8400. Also investigated was the effect of wall proximity on the calibration characteristics. Both types of probes have been used in subsequent programs; characteristic results are included.

PROBE GEOMETRIES

As the name implies, five-hole probes are characterized by five pressure sensing holes lying in two perpendicular planes with the line of intersection of the two planes passing through the central hole. Two different hole arrangements are diagrammed in Figures (1) and (2) where the pitch and yaw planes are also identified.

Five-hole probes are commercially available in several configurations; namely, spherical, conical, prismatic, etc. Five different probes that have been used at the ARL/PSU are shown in Figure (3). The primary emphasis in this paper will be placed on the results obtained while using the commercially available 0.125 inch (0.318 cm) diameter prism probe and the angle-tube probe. The angle-tube probes were fabricated at ARL/PSU according to the criteria presented in References [5] and [6]. The probe tip was made from five pieces of 0.050 inch (0.127 cm) diameter hypodermic tubing which had an assembled diameter of 0.150 inch (0.381 cm). The tubes were bonded together with soft solder. Tangential, epoxy fillets between the tubes were hand formed to acceptable hydrodynamic contours. A 0.250 inch (0.635 cm) diameter supporting member of circular cross section was chosen to avoid possible angle-of-attack errors which may be introduced with a more streamlined shape. The probe tip was located four support diameters upstream of this member to avoid support interference effects. The support was extended four support diameters beyond the tubing to improve the flow symmetry at the probe tip.

The geometry of the prism probe facilitates its use in turbomachinery research, since it can be easily inserted through casings and used

in studies where spatial restrictions are present. The geometry of the angle tube probes has generally limited their use to studies where the presence of flow boundaries has not been a problem.

CALIBRATION

Discussion

The five-hole probes employed in this study were used in a fixed position or non-nulling mode. This means that relationships must be determined between the measured pressures at the five holes and the true, local total and static pressure or velocity. These desired relationships are usually expressed as dimensionless pressure coefficients, which are functions of the flow angularity. Since, when in use, the flow angles are unknown, relationships between the five measured probe pressures and the flow direction are also required.

It would be advantageous if the calibration characteristics of a five-hole probe could be determined by analytical procedures. For probes of spherical geometry, a potential flow solution can predict the pressure distribution and the corresponding calibration characteristics to a reasonable accuracy. However, due to manufacturing inaccuracies and to operating range and accuracy requirements encountered in the laboratory or field conditions, calibrations are required for probes of this simple geometry. For probes of angle-tube or prismatic geometry, analytical procedures of any type are difficult. These complex geometries, characterized by abrupt changes in contour, are subject to viscous effects which are not modeled by current computational techniques. Thus, the only mathematical consideration at this stage is how to represent a given probe's response characteristics to a known flow field.

For operation in the non-nulling mode, it is apparent that the calibration characteristics must include data that represent pressure differences in both the pitch and yaw planes, Figures (1) and (2), as well as differences between the measured and the true local total and static pressures. The pressure coefficients representing these data must be defined so that they are independent of velocity and are a function only of the flow angularity. Krause and Dudzinski [5] found that an indicated dynamic pressure formed by the difference between the indicated total pressure, P_1, and the averaged value of the four indicated static pressures, P_2, P_3, P_4 and P_5, was a satisfactory normalizing parameter. It was demonstrated in Reference [6] that this normalizing parameter reduced the scatter in the calibration data as compared to using the true dynamic pressure. This is convenient, since using the true dynamic pressure would have introduced an unknown quantity. The four calibration coefficients are defined as follows:

$$*C_{P_{yaw}} = (P_2-P_3)/(P_1-\bar{P}) \tag{1}$$

$$C_{P_{pitch}} = (P_4-P_5)/(P_1-\bar{P}) \tag{2}$$

$$C_{P_{total}} = (P_1-P_{total})/(P_1-\bar{P}) \tag{3}$$

$$C_{P_{static}} = (\bar{P}-P_{static})/(P_1-\bar{P}) \tag{4}$$

$$\bar{P} = (P_2+P_3+P_4+P_5)/4 \quad . \tag{5}$$

The pitch and yaw planes are illustrated in Figures (1) and (2). Their

*all terms are defined in the nomenclature

orientation relative to the probe is dependent on the device used to position the probes during calibration. The "yaw-pitch" device shown in Figure (4) was used in a uniform flow field and permitted first a rotation of the probe about its longitudinal axis; i.e., a change in yaw angle, β. The probe was then tilted forward or backward providing a change in pitch angle, α. An alternate approach would be to use a "pitch-yaw" device which permitted a pitching motion followed by a yawing motion. Either approach is satisfactory if the user is consistent in the resolution of the velocity vectors, Figures (1) and (2). For both calibration and application, the probe's reference line is defined by some consistent characteristic of the probe's geometry. In application a reference direction obtained by balancing P_2 with P_3 and P_4 with P_5 is not always meaningful since initially a known flow direction would be required to relate the balanced condition to an absolute spatial reference.

Apparatus and Procedure

The previously discussed "yaw-pitch" calibration device, which is shown installed in the circular test section of the 12-inch diameter water tunnel, Figure (5), permitted a $\pm 30°$ rotation in both pitch and yaw. Because uniform flow fields were available in the 12-inch diameter water tunnel and an open jet facility, a more complex device which would have maintained the probe tip at a fixed location was not required. During the calibrations conducted in the open jet facility, precautions were taken to insure that the probes were located in the potential core of the jet. The velocity in the test section of the water tunnel and in the potential core of the jet, Reference [7],

had been shown by previous studies to be uniform within the accuracy of the experimental measurements.

A schematic diagram of the instrumentation for the open jet calibrations is shown in Figure (6). The reference total pressure was measured in the upstream settling section, and atmospheric pressure was used as the reference static pressure. A similar arrangement was used in the water tunnel calibrations except, the reference static pressure was recorded by a wall pressure tap in the test section.

To conduct the calibration of a given probe, the test velocity was maintained at a constant value. For calibration conducted in the 12.0-inch diameter water tunnel, the test section pressure was set at a value that was high enough to avoid cavitation at the probe tip. The probe was positioned at one of the predetermined yaw angles and then moved in prescribed increments through the pitch angle range. At each of the calibration points, the seven differential pressures indicated in Figure (6) were recorded and processed on an IBM 1130 computer. The data reduction program enabled the calculation of the four previously defined pressure coefficients, the test section velocity, and the Reynolds number based on the probe tip diameter. Each probe was calibrated three times; the resulting voltages were repeatable within two percent of the voltage corresponding to the maximum dynamic pressure. The final calibration characteristics were the mean values of the coefficients computed from the three individual runs. A statistical analysis of these data based on a typical probability curve indicated that the 90 percent error of the mean was less than 2.25 percent of the maximum value of each coefficient.

Results of the Calibrations

A complete set of calibration data for both probe geometries are presented in Figures (7), (8) and (9), where the graphical data have been represented by spline curves, Reference [8], passing through

the individual data points. Shown in Figure (7) are grids of $C_{p_{yaw}}$ versus $C_{p_{pitch}}$, where the nearly horizontal curves are curves of constant β and the nearly vertical curves are curves of constant α. Figures (8) and (9) show the variation of $C_{p_{static}}$ and $C_{p_{total}}$ with α for constant values of β.

Basically, the calibration data for the two probes are similar; the differences can be primarily attributed to geometric characteristics. One difference is indicated by the comparison of the two $C_{p_{pitch}}$ versus $C_{p_{yaw}}$ grids, which show that the prism probe has a much smaller range of $C_{p_{pitch}}$ values. This reduced range will result in an increased sensitivity of the prism probe to small flow variations in the pitch plane. The velocity component in this plane may, therefore, exhibit more data scatter.

The smaller range in $C_{p_{pitch}}$ is attributed to the different types of surfaces on which the holes in the two planes are located. At large yaw angles, one hole in the yaw plane is approximately aligned with the flow and senses pressures near the free-stream total pressure. The other hole senses a pressure much less than the free-stream static pressure, due to the acceleration of the flow around the probe. For the prism probe, however, the holes in the pitch plane have a different response. At large pitch angles, one hole again senses a pressure near the free-stream total pressure, whereas the other hole senses a pressure that is greater than the free-stream static pressure. This latter pressure may be higher due to a lower local acceleration and pressure recovery in the separated flow. Thus, the pressure difference sensed by the holes in the yaw plane exceed the difference measured by the holes in the

pitch plane. The resulting pressure coefficients reflect these differences.

The other major difference between the response of the two types of probes is that the Cp_{static} response of the prism probe, Figure (8), is somewhat skewed with respect to that of the angle-tube probe. The central hole of the prism probe is located only two probe diameters from its tip and is probably subject to complex end-flow effects. Whereas, the angle-tube probe had an extended support to improve flow symmetry.

Other repeatable nonsymmetries appearing in the data apparently resulted from the inability to fabricate a symmetric probe. Differences between the calibration characteristics of different probes of similar size and geometry were also observed. These observations emphasize the need to individually calibrate each probe.

All calibration data were repeatable within the two percent of the reference dynamic pressure when subjected to recalibration. These data consistently described the response of a particular probe, and thus, permit the successful application of the five-hole probes in a non-nulling mode.

APPLICATION

When used in the non-nulling mode of operation, the five-hole probe provides five pressure measurements via a differential pressure transducer. These pressures are usually recorded relative to some reference pressure, P_{ref}; i.e.,

$$\Delta P_i = P_i - P_{ref} \tag{6}$$

where the subscript "i" refers to the subject pressure. Local total and static pressure, pitch angle, yaw angle, and the three orthogonal velocity components can be computed from the probe data and the measured reference pressure. The interpolation procedures to perform these calculations have been computer-adapted and rely on the use of spline curves for all data specification.

The values of α and β are calculated from the grid of Cp_{yaw} versus Cp_{pitch}. The values to be determined from the calibration data are a function of two independent variables, and thus a double interpolation procedure is required. Using the measured data, Cp_{yaw} and Cp_{pitch} can be calculated from Equations (1) and (2). These experimental coefficients are represented by the "primed" superscripts, i.e., $C'_{p_{yaw}}$ and $C'_{p_{pitch}}$. Individual spline curves are passed through the Cp_{yaw} versus Cp_{pitch} calibration data for each value of β. At $C'_{p_{pitch}}$, the corresponding values of Cp_{yaw} are interpolated from the spline curves yielding the variation of β versus Cp_{yaw}. This resulting monotonically increasing function, when evaluated at

$C_{P_{yaw}}'$, yields the experimental local flow angle in the yaw plane, β'. By interchanging the dependent and independent variables and forming the functional relationship between α and $C_{P_{pitch}}$ for a constant value of $C_{P_{yaw}}'$, the experimental value of the local pitch angle, α', can be determined.

From α' and β' the experimental value of the static pressure coefficient, $C_{P_{static}}'$, is obtained from the second part of the calibration data. Individual spline curves are passed through the $C_{P_{static}}$ versus α data for each value of β. At α', the corresponding values of $C_{P_{static}}$ are interpolated from the spline curves yielding the variation of $C_{P_{static}}$ versus β. When the resulting curve is evaluated at β', the experimental value of the static pressure coefficient, $C_{P_{static}}'$, results. The experimental value of the total pressure coefficient, $C_{P_{total}}'$, is evaluated in the same manner using the third graph of the calibration data.

When the absolute value of the reference pressure is recorded, the total and static pressures at the probe tip can be computed from $C_{P_{total}}$ and $C_{P_{static}}$, respectively.

$$C_{P_{total}}' = (\Delta P_1 - \Delta P_t)/(\Delta P_1 - \overline{\Delta P}) \tag{7}$$

and

$$\Delta P_t = P_{total} - P_{ref} \quad . \tag{8}$$

Thus,

$$P_{total} = P_{ref} + \Delta P_1 - C_{P_{total}}'(\Delta P_1 - \overline{\Delta P}) \quad . \tag{9}$$

In Equation (9), all terms on the right of the equal sign are measured values except for $C_{P_{total}}'$ which was determined from the calibration data. In a similar manner, the static pressure is computed as

$$P_{static} = P_{ref} + \overline{\Delta P} - C_{P_{static}}'(\Delta P_1 - \overline{\Delta P}) \quad . \tag{10}$$

By using Bernoulli's equation, the magnitude of the local total velocity vector is

$$\overline{V} = \sqrt{\frac{2}{\rho}(P_{total} - P_{static})} \quad . \tag{11}$$

By proper manipulation of the above equations, $\overline{V}$ could also be calculated directly from $C_{P_{total}}'$ and $C_{P_{static}}'$.

$$\overline{V} = \{(2/\rho)(\Delta P_1 - \overline{\Delta P})(1 + C_{P_{static}}' - C_{P_{total}}')\}^{1/2} \quad . \tag{12}$$

When Reynolds number or wall proximity effects are present, they are included as corrections to the calculated static pressure coefficients.

The manner by which the velocity is resolved is dependent upon the order of rotation employed during the calibration, i.e., upon the type of probe holder employed. The two corresponding sets of equations are presented in Figures (1) and (2) where the spatial orientation of the velocity vectors are illustrated. A more mathematically rigorous approach to the velocity resolution is discussed in Appendix A.

THE EFFECTS OF REYNOLDS NUMBER ON THE CALIBRATION DATA

Meaningful calibration data should be independent of the measured quantities. In most five-hole probe applications, velocity is the primary parameter to be measured; thus, the effect of changes in Reynolds number, R_n, on the calibration data should be evaluated. To investigate these effects the prism probes were calibrated in the open jet facility over an R_n range of 2000 to 7000. The angle-tube probes were calibrated in the water tunnel at R_n=20,000 and in the open jet facility at R_n=8400.

For both types of five-hole probes the total pressure, pitch and yaw coefficients were essentially uneffected by the Reynolds number variation. Whereas, a measurable change in the static pressure coefficient was observed for both probe geometries. Typical results for the prism probes are shown in Figures (10) and (11). As an example, the effect of an R_n variation from 3000 to 7000 at α=30, β=20 is shown to produce a maximum change in measured static pressure of 5.5 percent of the dynamic head and a 2.8 percent change in the velocity measurement.

To account for the dependency of the static pressure coefficient on the Reynolds number, a three parameter calibration in terms of α, β, and R_n would be necessary. In application, a corresponding iterative procedure in terms of the unknown R_n would be required. These complications limit the practicality of the probes if they are to be used in studies characterized by large R_n variations. However, several approaches are possible: one is to calibrate at the expected Reynolds number, another is to determine correction factors from the calibration data and to apply these as average values over small R_n ranges. This latter

approach is justified due to the relatively weak dependence of Cp_{static} on R_n. Both of these approaches are currently being employed.

WALL PROXIMITY EFFECTS ON THE CALIBRATION DATA

The experimental investigation of wall proximity effects on the calibration characteristics of the prism probes was conducted in the presence of a sharp-edged flat plate that spanned the working area of the open jet facility. With the flat plate mounted parallel to the flow and with the measuring station located 5.0 inches (12.7 cm) downstream of the leading edge, the local boundary-layer thickness was small compared to the probe diameter. Thus, any changes in the calibration characteristics in the proximity of the plate were attributed to a probe-plate potential flow interaction as opposed to boundary-layer effects. It should be noted that errors in boundary-layer measurements are primarily a function of the local velocity gradient and the size and spacing of the holes. This implies that the problem in boundary-layer measurements is one of probe selection and not one of calibration.

Calibrations were conducted at R_n=7000 for the probe both approaching and being withdrawn through the plate. For both installations, β was varied from -30° to +30° at each of the selected measuring points while maintaining α=0° and a perpendicular probe-plate orientation.

These latter restrictions were necessary; since, with the present apparatus, it was impossible to change the flow angle, α, without also altering the orientation of the probe with respect to the plate. Although the effects caused by a wall may be a function of both α and β as well as the distance to the wall, the pitch angle could not be varied without introducing the probe-plate orientation as an additional variable. Thus, to apply the wall effects data the

assumption must be made that the probe response is independent of pitch angle. This assumption appears reasonable from observations of the available data. Figures (12) and (14) show that the changes in calibration data as a function of distance are quite similar for the various yaw angles tested. This suggests that the wall proximity effects are primarily a function of distance only. Additional investigations in this area would require an apparatus capable of changing α while maintaining the same probe-like orientation. For calibrations with the probe approaching the plate, only the static pressure coefficient was altered. A representative variation of Cp_{static} with probe-to-plate spacing is shown in Figure (12). For the other configuration in which the probe was withdrawn through the plate, all calibration coefficients were altered within two probe diameters of the plate. These effects are illustrated by the Cp_{yaw} and Cp_{static} data shown in Figures (13) and (14), respectively. This observed variation in all coefficients makes these probes essentially impractical for measurements when the center hole is within two probe diameters of the wall. Thus, a limitation of two probe diameters is imposed as the probe is withdrawn through a wall; whereas the probe's geometry imposes a physical limitation of the same magnitude as the probe approaches a wall.

Restricting the use of the probe to distances greater than two probe diameters does not eliminate all wall interaction effects. Figures (12) and (14) show that Cp_{static} is still affected at greater distances.

These effects of the wall, when limited to Cp_{static} only, can be incorporated in the data reduction program in a similar manner to that used for the Reynolds number effects.

EXPERIMENTAL APPLICATION

As implied by previous statements, the five-hole probes were first applied at ARL/PSU to measure the three-dimensional wake occurring in the propeller plane of a surface ship model. In this case six individually calibrated angle-tube probes were assembled in a rotating wake rake as shown in Figure (15). Typical results of a circumferential survey at one radial position are presented in Figure (16) and compared with towing tank data obtained using a 0.375 inch (0.952 cm) diameter spherical five-hole probe.

Presented in Figure (17) are the results of boundary layer surveys conducted in air on an elliptic body of revolution. These surveys were made with a boundary layer rake, a hot wire sensor, and a 0.125 inch (0.318 cm) diameter prism probe. Additional comparative data are shown in Figure (18), where the flow immediately downstream of a rotating blade row was surveyed with both a laser doppler velocimeter and a prism probe.

SUMMARY

Probes of angle-tube design manufactured at ARL/PSU and commercially available prism probes were calibrated in the 12-inch diameter water tunnel and the open air jet facility. The probes were individually mounted in a calibration device which permitted a ±30° variation in both pitch and yaw angle with respect to the known velocity. The response coefficient measured at each angular settling, when mathematically connected by spline curves, defined the calibration grids for each probe.

For calibrations of this type to be meaningful, the calibration data must be repeatable and independent of the measured quantities. Each probe was calibrated three times to demonstrate the repeatability of the data and to permit the averaging of the data to further reduce the minimal data scatter. Additional measurements were conducted to assess the influence of Reynolds number on the calibration data. For the range of Reynolds number employed, no effect was measured on the pitch, yaw, or total pressure coefficients; whereas, the static pressure coefficient showed sufficient change to cause minor variations in the magnitude of the calculated velocity vector. However, average correction factors were incorporated into the data reduction procedures to account for these variations in the static pressure coefficients.

Also investigated was the effect of wall proximity on the calibration data obtained for the prism probe. Calibrations were conducted for a probe approaching normal to a flat plate that had been aligned parallel

to the reference flow. Only the static pressure coefficient exhibited significant changes. For the probe being withdrawn through the plate, all calibration coefficients were altered with two probe diameters of the wall; however, at distances greater than two probe diameters from the wall, only the static pressure coefficient was influenced. These wall interference corrections were also incorporated in the final data reduction program which uses a spline curve interpolation procedure to calculate the three cylindrical velocity components from the five measured pressures.

The probes have been used to survey the three-dimensional flow fields in the propeller-planes of surface ships, as well as in the inlet and exit planes of other rotating blade rows. These results agreed well with data measured by other types of probes and velocity measuring instrumentation.

References

[1] Janes, C. E., "Instruments and Methods for Measuring the Flow of Water Around Ships and Ship Models," David Taylor Model Basin Report 487, March 1948.

[2] Pien, P. C., "Five-Hole Spherical Pitot Tube," David Taylor Model Basin Report 1229, May 1958.

[3] Lehman, A. F., "The Garfield Thomas Water Tunnel," ORL TM NOrd 16597-56, September 1959.

[4] Treaster, A. L. and Eisenhuth, J. J., "Surface Ship Testing at the Garfield Thomas Water Tunnel," ARL TM 77-212, June 1977.

[5] Krause, L. N. and Dudzonski, T. J., "Flow-Direction Measurement with Fixed Position Probes in Subsonic Flows over a Range of Reynolds Numbers," NASA TMX-52576, May 1969.

[6] Gettelman, C. C. and Krause, L. N., "Considerations Entering into the Selection of Probes for Pressure Measurements in Jet Engines," ISA Proc. 1, 134-137, 1952.

[7] Nilsen, A. W., "Analysis of the Unsteady Pressures in a Turbulent Jet," M. S. Thesis in Aerospace Engineering at The Pennsylvania State University, September 1969.

[8] Davis, R. F., "Spline Curve Fit Functions, Their Derivation and Use," ORL TM 512.3531-02, July 1968.

[9] Yeh, H. and Abrams, J. I., Mechanics of Solids and Fluids, Vol. 1, Chapter 11, McGraw-Hill Book Co., Inc., 1960.

Appendix A

Vector Resolution

In this appendix an analytical development of the vector resolution equations shown in Figures (1) and (2) is presented. The question to be answered is: What are the R, θ and X components of a vector $\overline{V}$ at angles α and β with respect to the local probe axes? From Figures (1) and (2) it is obvious that this question has two answers which depend on the definition of the pitch angle α and the yaw angle β. Defined in Figure (1) is the relationship between α, β and $\overline{V}$ resulting from calibrations where the first rotation was in the yaw-plane followed by rotation in the pitch-plane (yaw-pitch mode). The alternate rotational procedure (pitch-yaw mode) is defined in Figure (2). For either mode of operation the resulting equations can be developed from the orthogonal transformation procedure discussed in Reference [10].

Consider any vector $\overline{V}$ whose components are V_1, V_2, V_3 in the original, or unprimed coordinate system and V_1', V_2', V_3' in the primed or rotated coordinate system. It can be shown that the primed components can be computed from

$$V_i' = \sum_j a_{ij} V_j \qquad (1A)$$

where the a_{ij}'s are the diretion cosines defined by

$$a_{ij} = \cos(X_i', X_j) \quad . \qquad (2A)$$

The symbol (X_i', X_j) represents the angle between the positive direction of the axes X_i' and X_j. The vector resolution for data obtained from

probes that were calibrated in the yaw-pitch mode will be examined first.

Vector Resolution for Probes Calibrated in the Yaw-Pitch Mode

Let $\overline{V}$ be the reference velocity in the positive X_3 direction of the original axes system; i.e., V_1=0.0; V_2=0.0 and $V_3=\overline{V}$. The first rotation is a yawing motion about the X_1 axis of magnitude β. The goemetry is illustrated in Figure (1A).

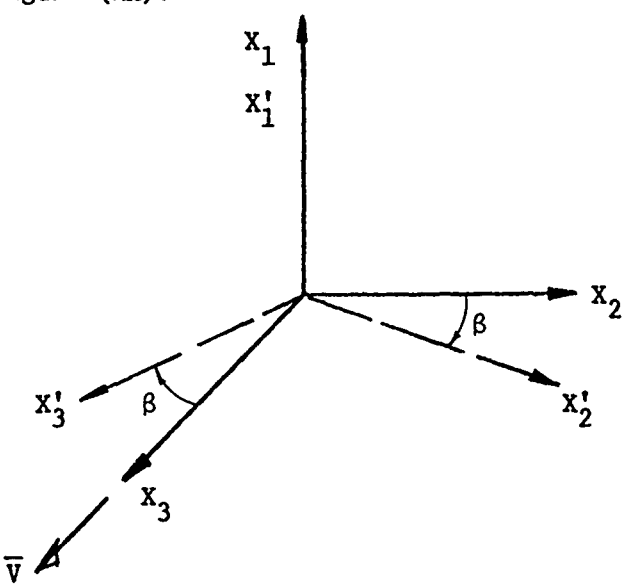

Figure (1A)

Thus,

$$\left.\begin{aligned}
a_{11} &= \cos(X_1', X_1) = \cos(0°) = 1.0 \\
a_{21} &= \cos(X_2', X_1) = \cos(90°) = 0.0 \\
a_{31} &= \cos(X_3', X_1) = \cos(90°) = 0.0 \\
a_{12} &= \cos(X_1', X_2) = \cos(90°) = 0.0 \\
a_{22} &= \cos(X_2', X_2) = \cos(\beta) = \cos\beta \\
a_{32} &= \cos(X_3', X_2) = \cos(90°+\beta) = -\sin\beta \\
a_{13} &= \cos(X_1', X_3) = \cos(90°) = 0.0 \\
a_{23} &= \cos(X_2', X_3) = \cos(90°-\beta) = \sin\beta \\
a_{33} &= \cos(X_3', X_3) = \cos\beta
\end{aligned}\right\} \quad (3A)$$

From Equation (1A) the components of $\overline{V}$ in the rotated axes system are

$$V_1' = a_{11} V_1 + a_{12} V_2 + a_{13} V_3 = 0.0 \tag{4A}$$

$$V_2' = a_{21} V_1 + a_{22} V_2 + a_{23} V_3 = \overline{V} \sin\beta \tag{5A}$$

$$V_3' = a_{31} V_1 + a_{32} V_2 + a_{33} V_3 = \overline{V} \cos\beta \quad . \tag{6A}$$

For the yaw-pitch calibration the next rotation is a pitching motion about the X_2' axis of magnitude α. This final axes orientation will be denoted by the double primed symbols. The geometry is shown in Figure (2A).

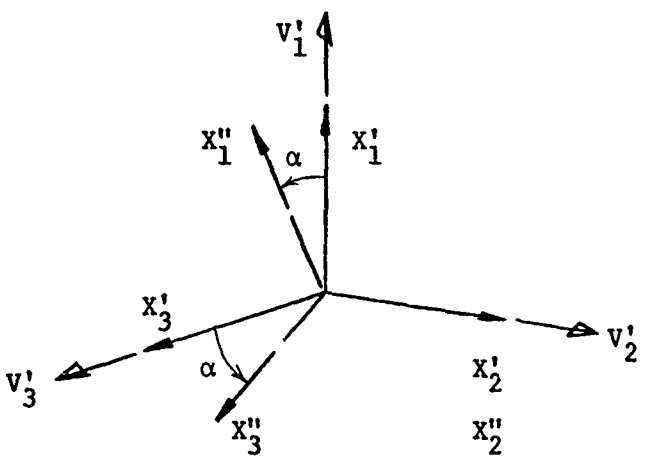

Figure (2A)

$$\left.\begin{aligned}
a_{11} &= \cos(X_1'', X_1') = \cos\alpha \\
a_{21} &= \cos(X_2'', X_1') = \cos(90°) = 0.0 \\
a_{31} &= \cos(X_3'', X_1') = \cos(90+\alpha) = -\sin\alpha \\
a_{12} &= \cos(X_1'', X_2') = \cos(90) = 0.0 \\
a_{22} &= \cos(X_2'', X_2') = \cos(0) = 1.0 \\
a_{32} &= \cos(X_3'', X_2') = \cos(90) = 0.0 \\
a_{13} &= \cos(X_1'', X_3') = \cos(90-\alpha) = \sin\alpha \\
a_{23} &= \cos(X_2'', X_3') = \cos(90°) = 0.0 \\
a_{33} &= \cos(X_3'', X_3') = \cos\alpha
\end{aligned}\right\} \quad . \tag{7A}$$

The components V_1', V_2'', V_3'' of the original vector $\bar{V}$ relative to the final axes orientation are obtained by combining Equations (4A) through (7A) via Equation (1A).

$$V_1'' = a_{11} V_1' + a_{12} V_2' + a_{13} V_3' = \bar{V} \cos\beta \sin\alpha \quad (8A)$$

$$V_2'' = a_{21} V_1' + a_{22} V_2' + a_{23} V_3' = \bar{V} \sin\beta \quad (9A)$$

$$V_3'' = a_{31} V_1' + a_{32} V_2' + a_{33} V_3' = \bar{V} \cos\beta \cos\alpha \quad . \quad (10A)$$

In many applications these three velocity components are identified as follows:

$$V_R = V_1'' = \bar{V} \cos\beta \sin\alpha \quad (11A)$$

$$V_\theta = V_2'' = \bar{V} \sin\beta \quad (12A)$$

$$V_x = \bar{V} \cos\beta \cos\alpha \quad . \quad (13A)$$

For surface ship applications V_R is positive when directed radially inward along the longitudinal probe axis; V_θ is positive when directed counter-clockwise when looking upstream; and V_x is positive in the axial direction as shown in Figures (1) and (2). In Figures (1A) and (2A) the direction of rotation was chosen so that positive vector components resulted.

Vector Resolution for Probes Calibrated in the Pitch-Yaw Mode

The previous procedure is continued in this section; only the order of rotation is changed. The first rotation is a pitching motion about the X_2 axis of magnitude α. Again, $\bar{V}$ is the reference velocity which has $\bar{V}_3$ as its only nonzero component. The geometry is shown in Figure (3A).

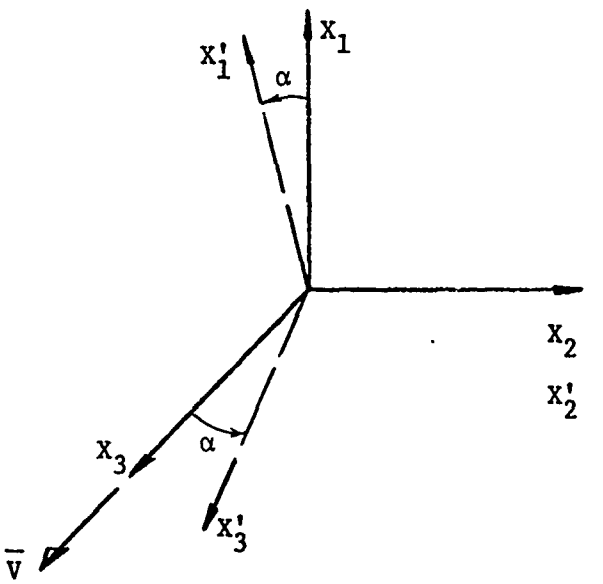

Figure (3A)

Since V_1 and V_2 are both zero

$$V_1' = a_{13} V_3 = \cos(90°-\alpha)V_3 = \bar{V} \sin\alpha \quad (14A)$$

$$V_2' = a_{23} V_3 = \cos(90°)V_3 = 0.0 \quad (15A)$$

$$V_3' = a_{33} V_3 = \bar{V} \cos\alpha \quad . \quad (16A)$$

For the pitch-yaw calibration the next rotation is a yawing motion about the X_1' axis of magnitude β. The final axes orientation is denoted by the double primed symbols in Figure (4A).

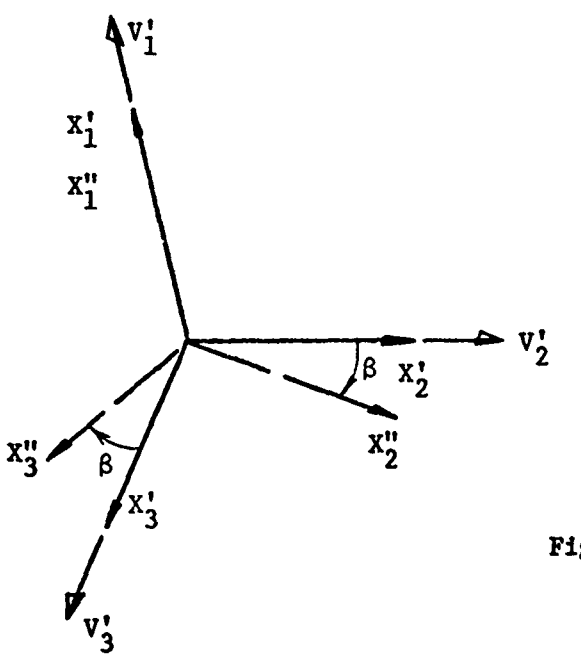

Figure (4A)

$$\left.\begin{aligned} a_{11} &= \cos(0) = 1.0 \\ a_{21} &= \cos(90°) = 0.0 \\ a_{31} &= \cos(90°) = 0.0 \\ a_{12} &= \cos(90°) = 0.0 \\ a_{22} &= \cos\beta \\ a_{32} &= \cos(90+\beta) = -\sin\beta \\ a_{13} &= \cos(90°) = 0.0 \\ a_{23} &= \cos(90-\beta) = \sin\beta \\ a_{33} &= \cos\beta \end{aligned}\right\} \quad . \tag{17A}$$

As before, the components V_1'', V_2'', V_3'' of the original vector $\overline{V}$ relative to the final axes orientation are obtained by combining Equations (14A) through (17A) via Equation (1A).

$$V_1'' = \overline{V} \sin\alpha \tag{18A}$$

$$V_2'' = \overline{V} \cos\alpha \sin\beta \tag{19A}$$

$$V_3'' = \overline{V} \cos\alpha \cos\beta \quad . \tag{20A}$$

In more usual terminology

$$V_R = V_1'' = \overline{V} \sin\alpha \tag{21A}$$

$$V_\theta = V_2'' = \overline{V} \cos\alpha \sin\beta \tag{22A}$$

$$V_x = V_3'' = \overline{V} \cos\alpha \cos\beta \quad . \tag{23A}$$

Thus, it has been demonstrated that two different sets of data reduction equations are required by the two calibration procedures.

Fig. 1 - GEOMETRY OF THE ANGLE-TUBE PROBES

VECTOR RESOLUTION FOR A PROBE CALIBRATED IN THE YAW-PITCH MODE

$V_x = \bar{V} \cos\beta \cos\alpha$

$V_R = \bar{V} \cos\beta \sin\alpha$

$V_\theta = \bar{V} \sin\beta$

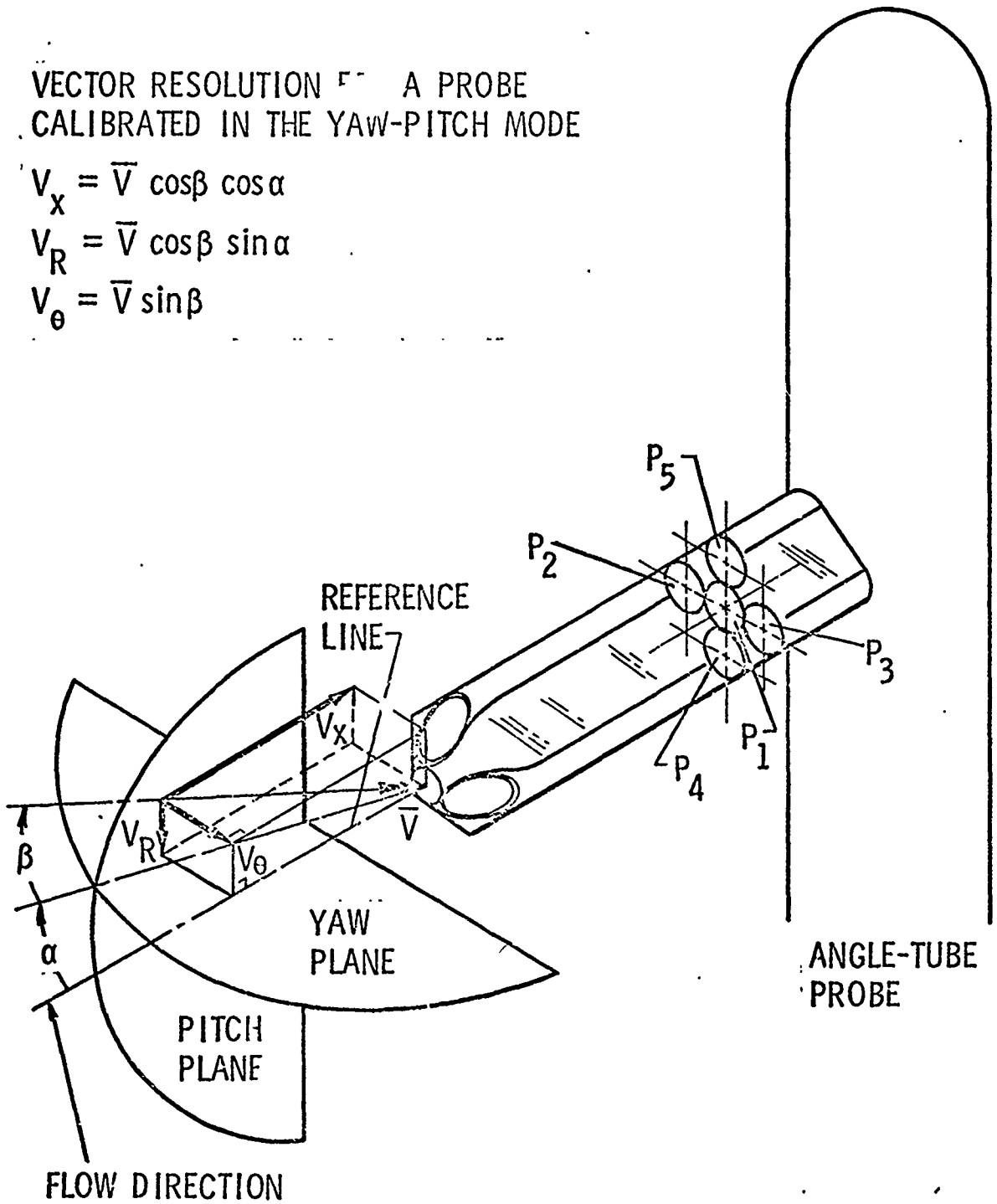

VECTOR RESOLUTION FOR A PROBE
CALIBRATED IN THE PITCH-YAW MODE

$V_x = \bar{V} \cos\alpha \cos\beta$

$V_R = \bar{V} \sin\alpha$

$V_\theta = \bar{V} \cos\alpha \sin\beta$

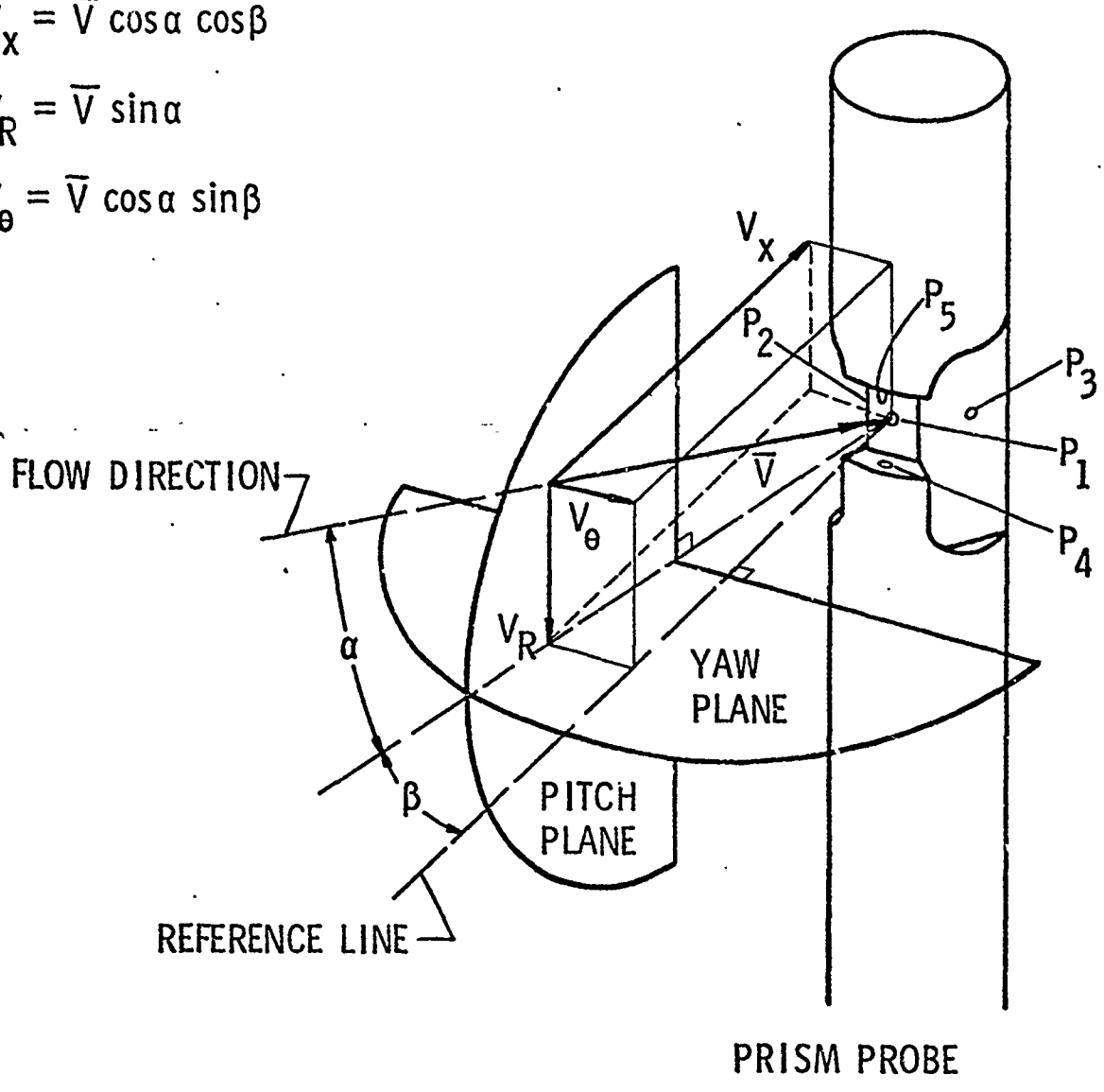

Fig. 2 - GEOMETRY OF THE PRISM PROBES

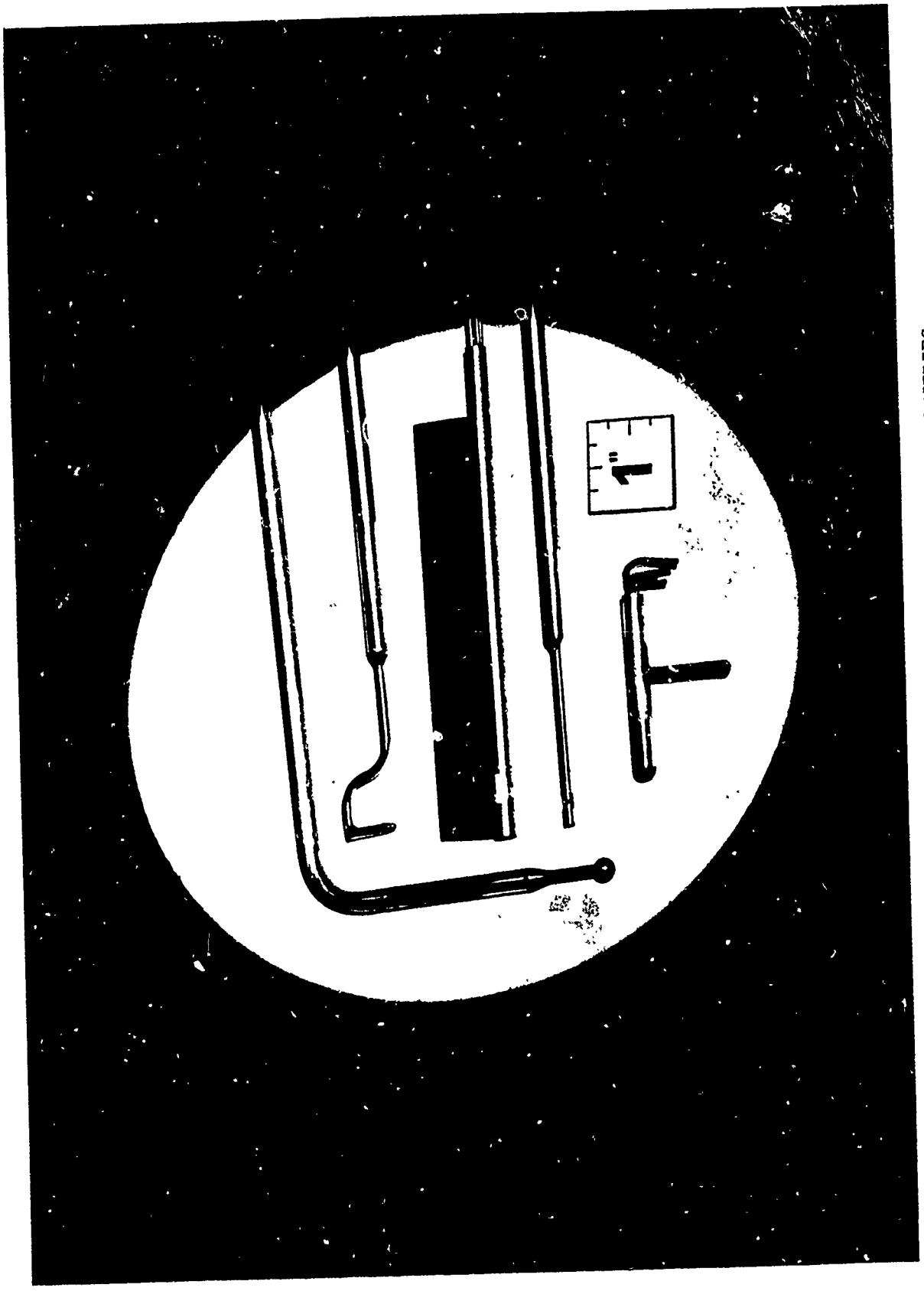

Fig. 3 - TYPICAL FIVE-HOLE PROBE GEOMETRIES

Fig. 4 - THE YAW-PITCH CALIBRATION DEVICE

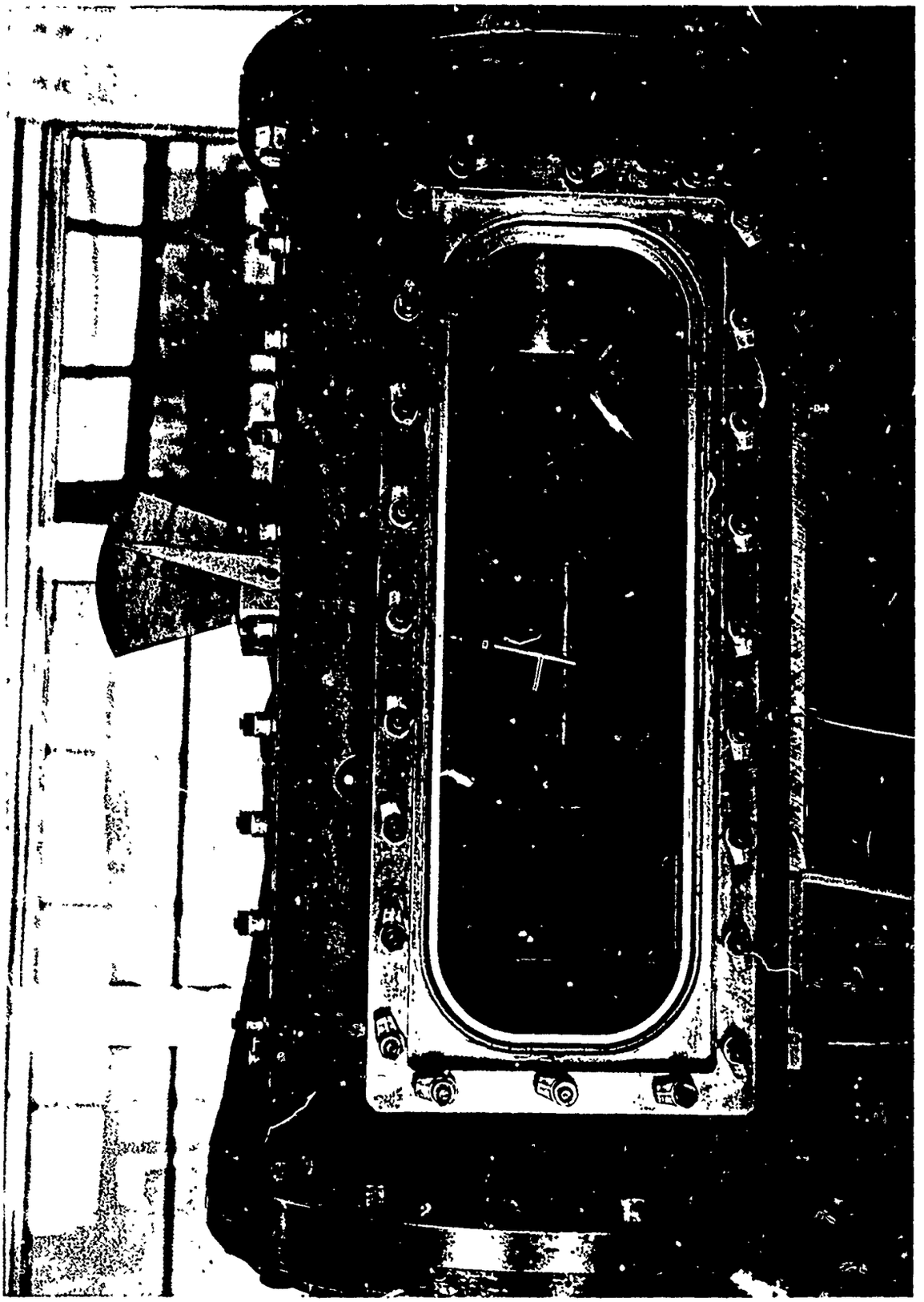

Fig. 5 - WATER TUNNEL CALIBRATION

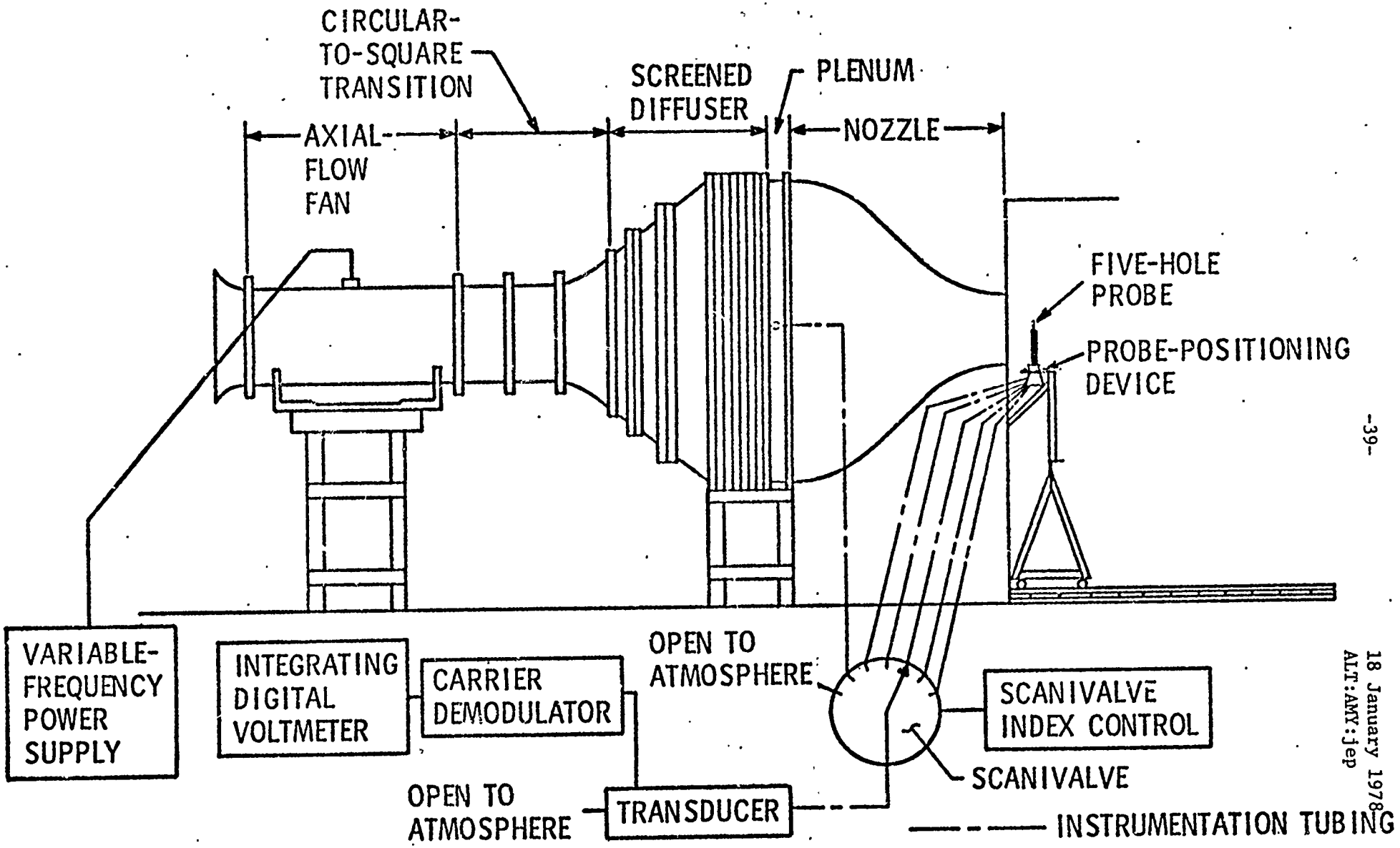

Fig. 6 - CALIBRATION SCHEMATIC (OPEN JET FACILITY)

18 January 1978
ALT:AMY:jep

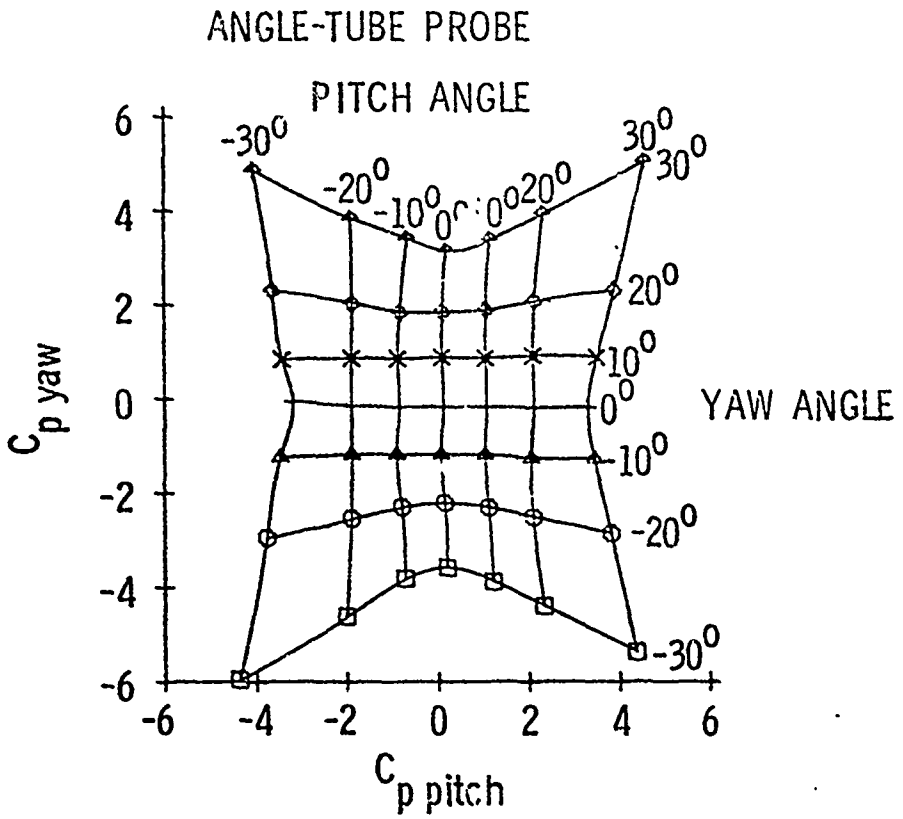

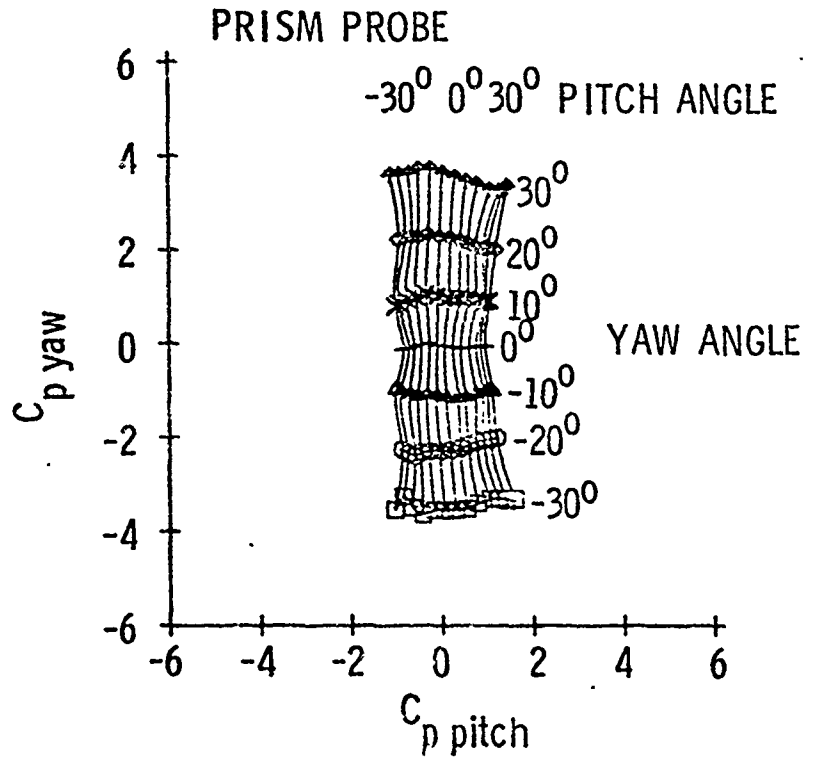

Fig. 7 - TYPICAL CALIBRATION DATA
$C_{p\ yaw}$ vs $C_{p\ pitch}$

18 January 1978
ALT:AMY:jep

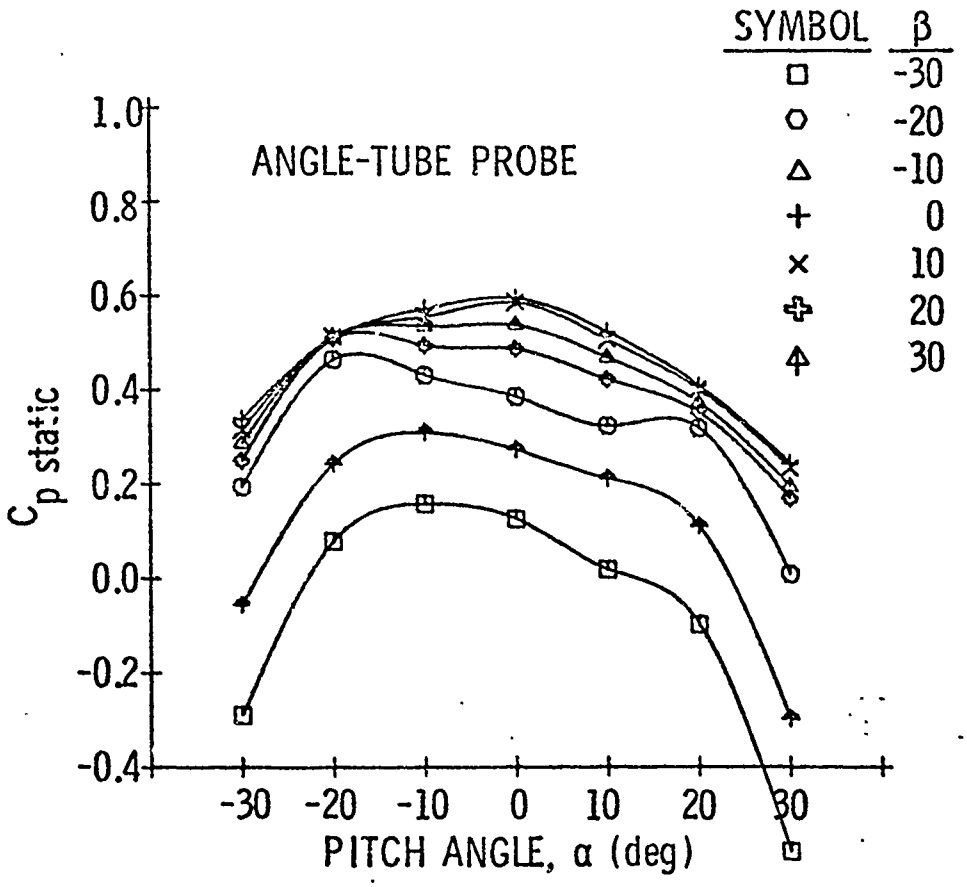

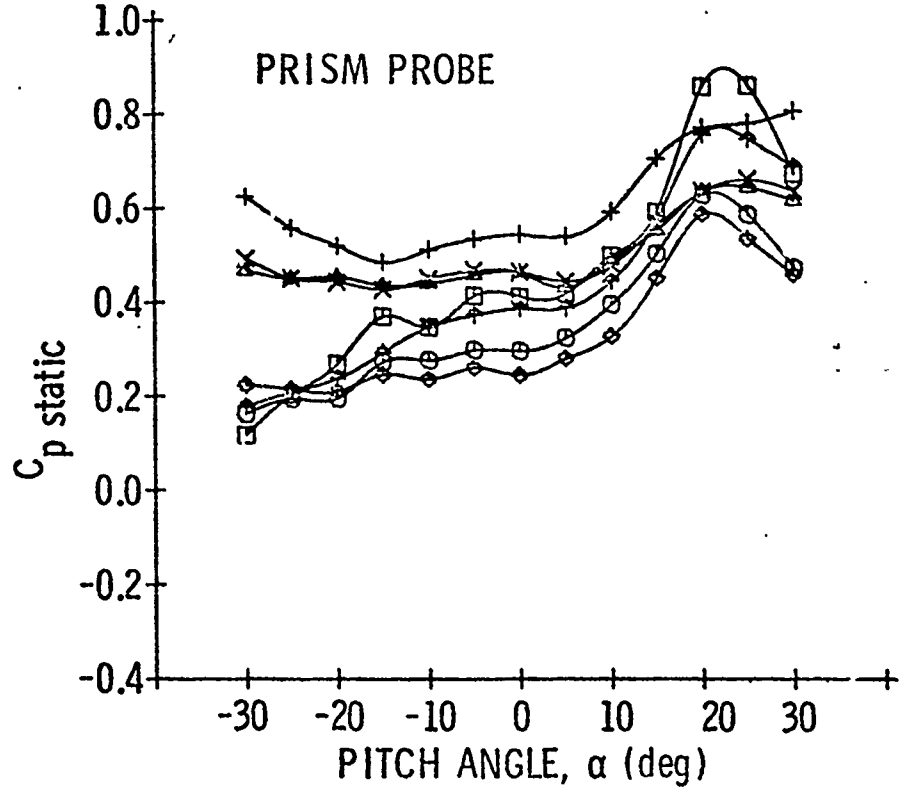

Fig. 8 - TYPICAL CALIBRATION DATA
$C_{p\ static}$ vs α

18 January 1978
ALT:AMY:jep

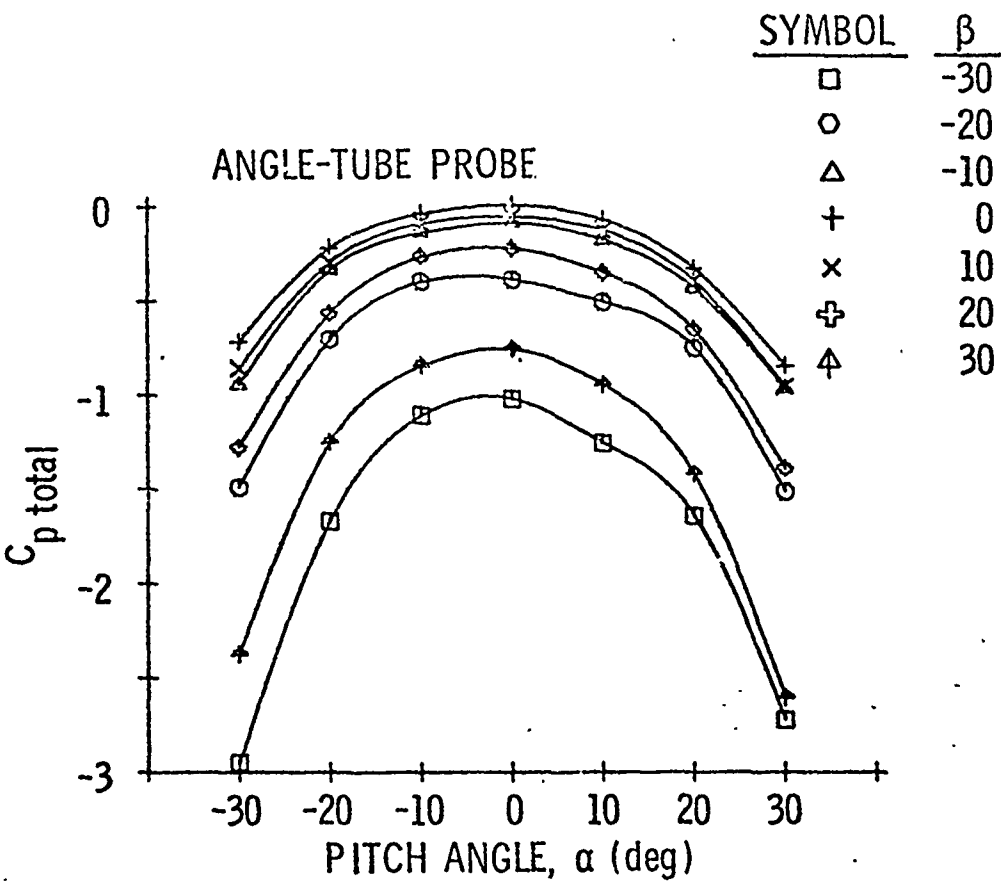

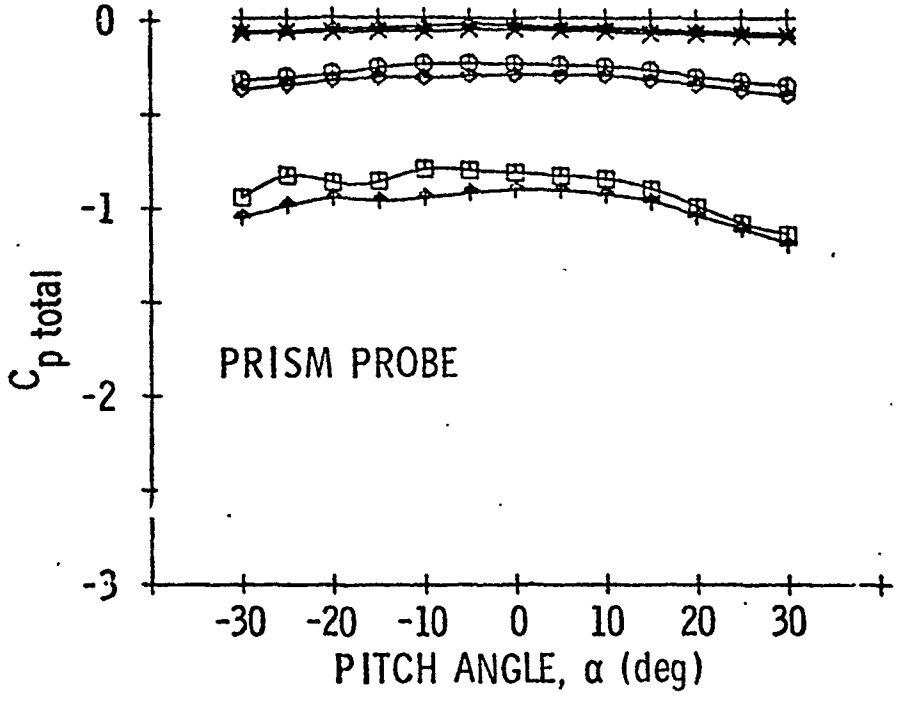

Fig. 9 - TYPICAL CALIBRATION DATA
$C_{p\ total}$ vs α

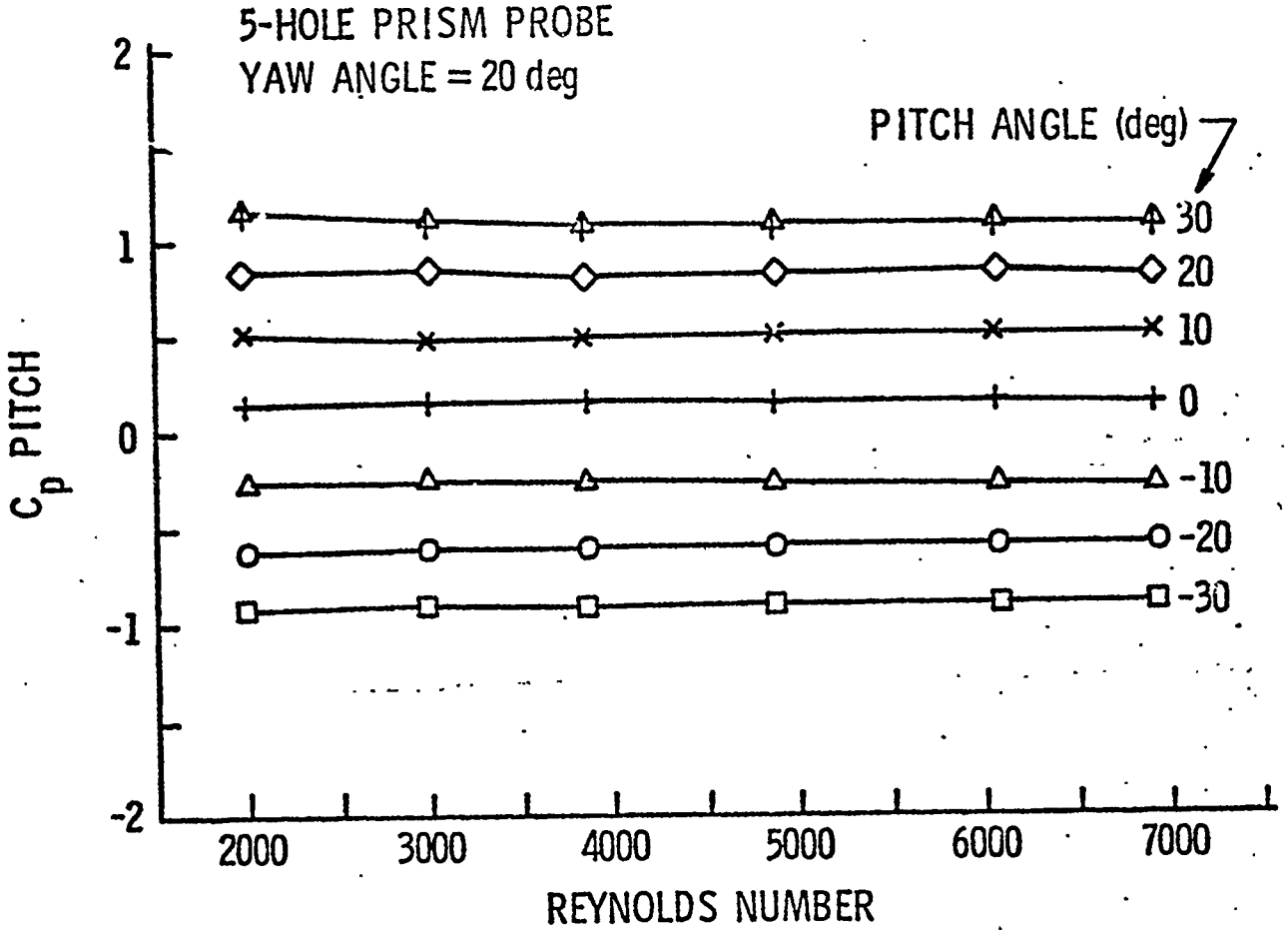

Fig. 10 - TYPICAL REYNOLDS NUMBER EFFECT ON THE CALIBRATION DATA ($C_{p\ pitch}$)

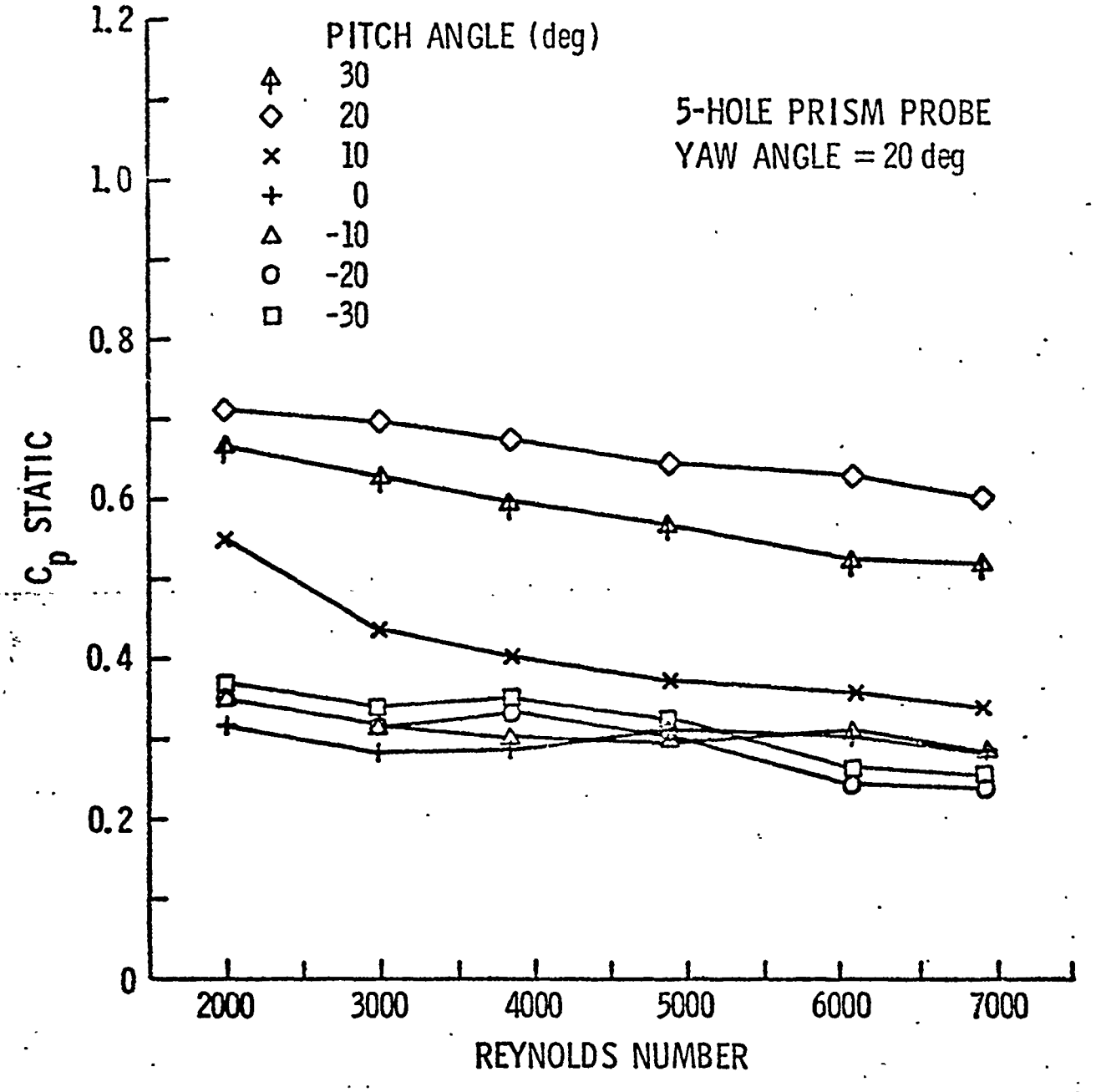

Fig. 11 - TYPICAL REYNOLDS NUMBER EFFECTS ON THE CALIBRATION DATA ($C_{p\ static}$)

18 January 1978
ALT:AMY:jep

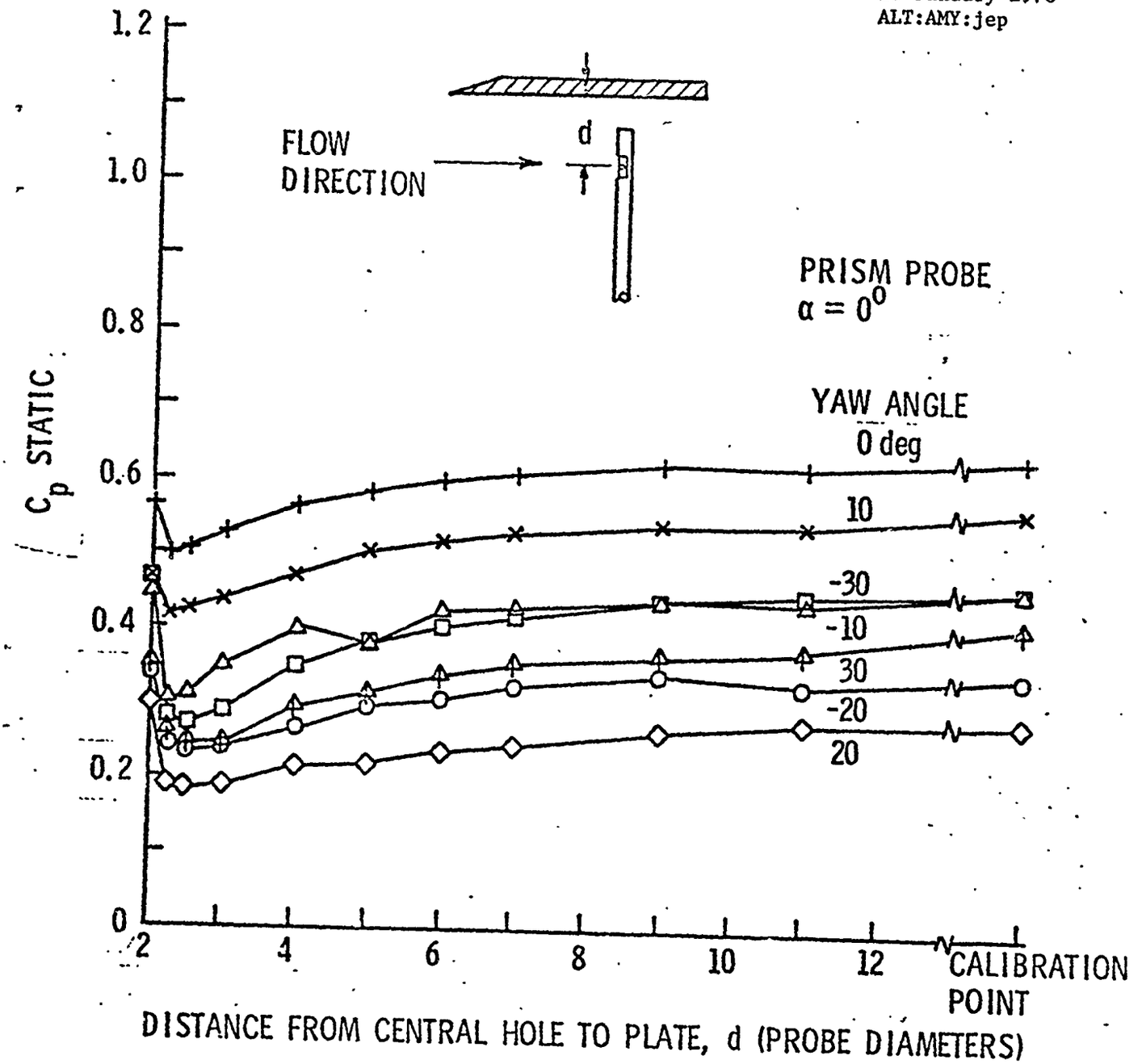

Fig. 12 - TYPICAL WALL PROXIMITY EFFECTS ON THE CALIBRATION DATA

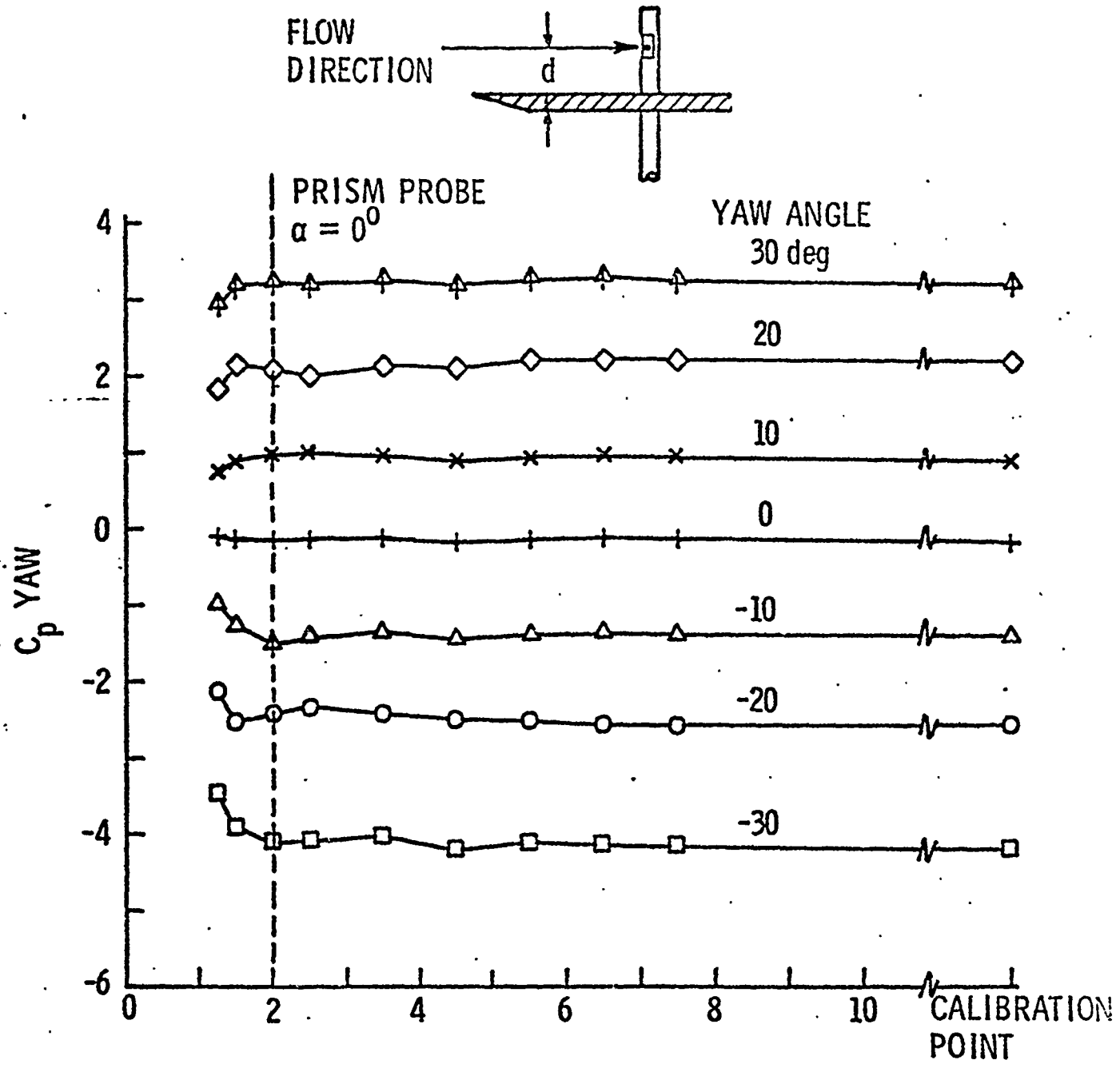

Fig. 13 - TYPICAL WALL PROXIMITY EFFECTS ON THE CALIBRATION DATA

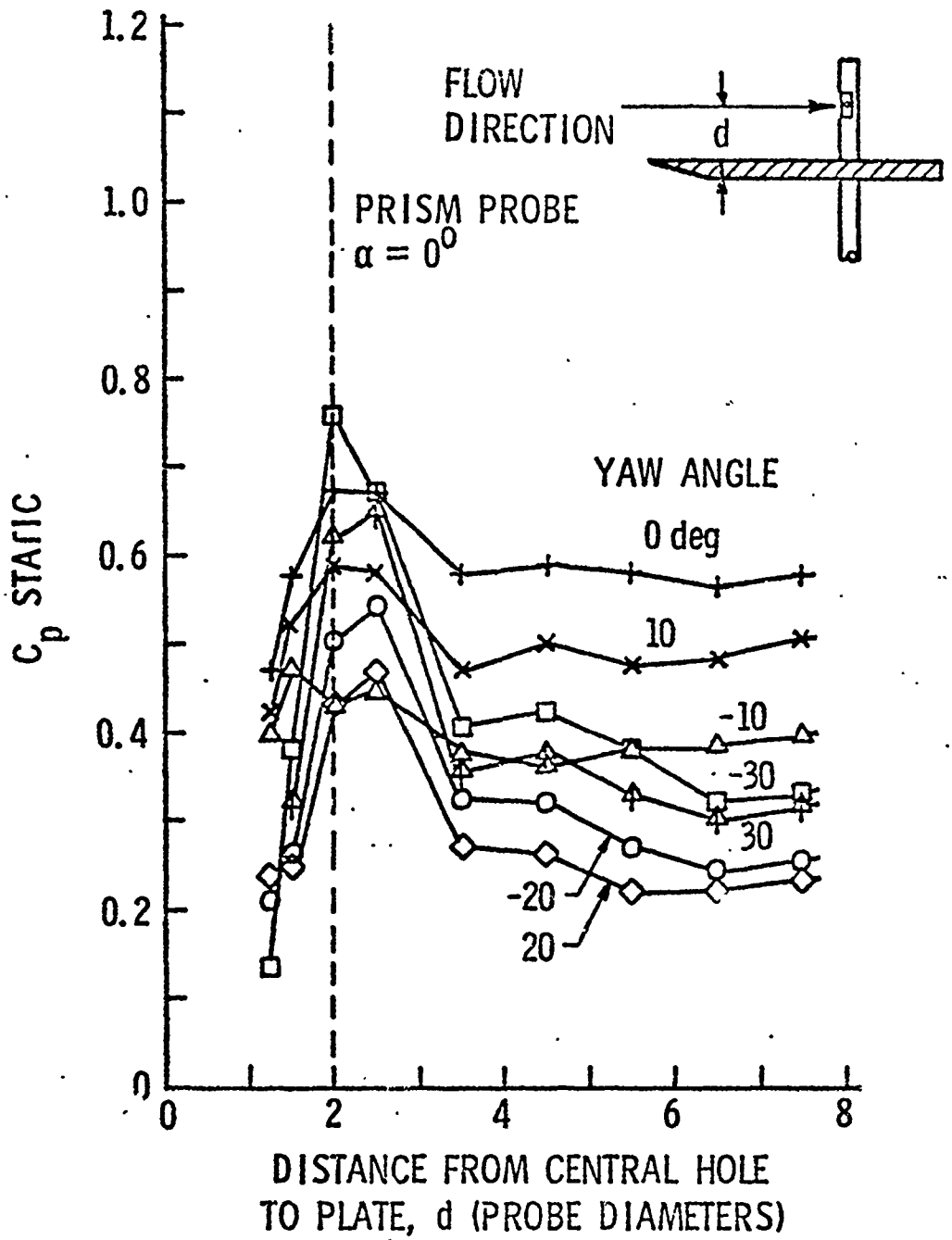

Fig. 14 - TYPICAL WALL PROXIMITY EFFECTS ON THE CALIBRATION DATA

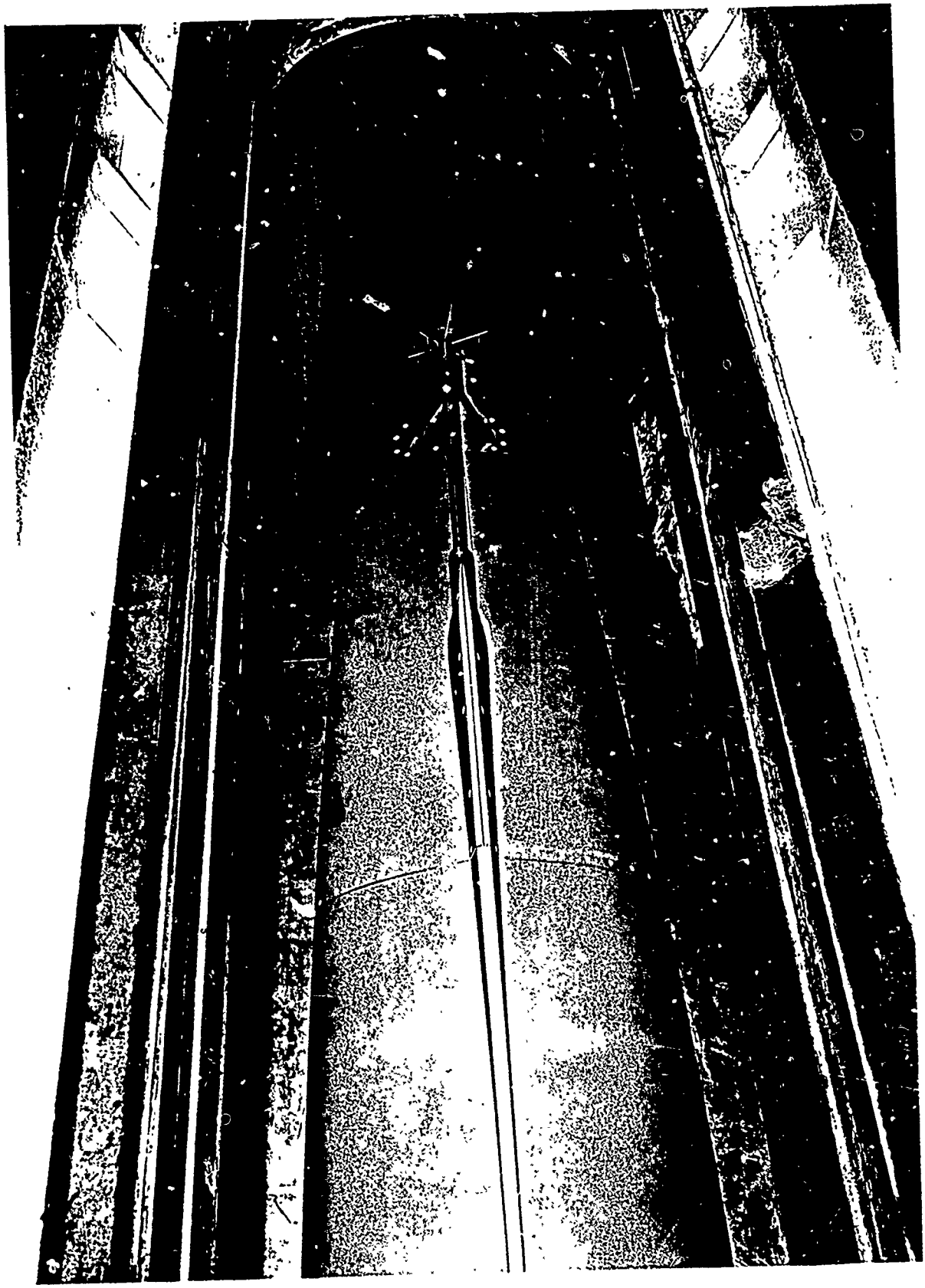

Fig. 15 - ROTATING FIVE-HOLE PROBE WAKE RAKE INSTALLED ON THE MODIFIED SURFACE SHIP MODEL

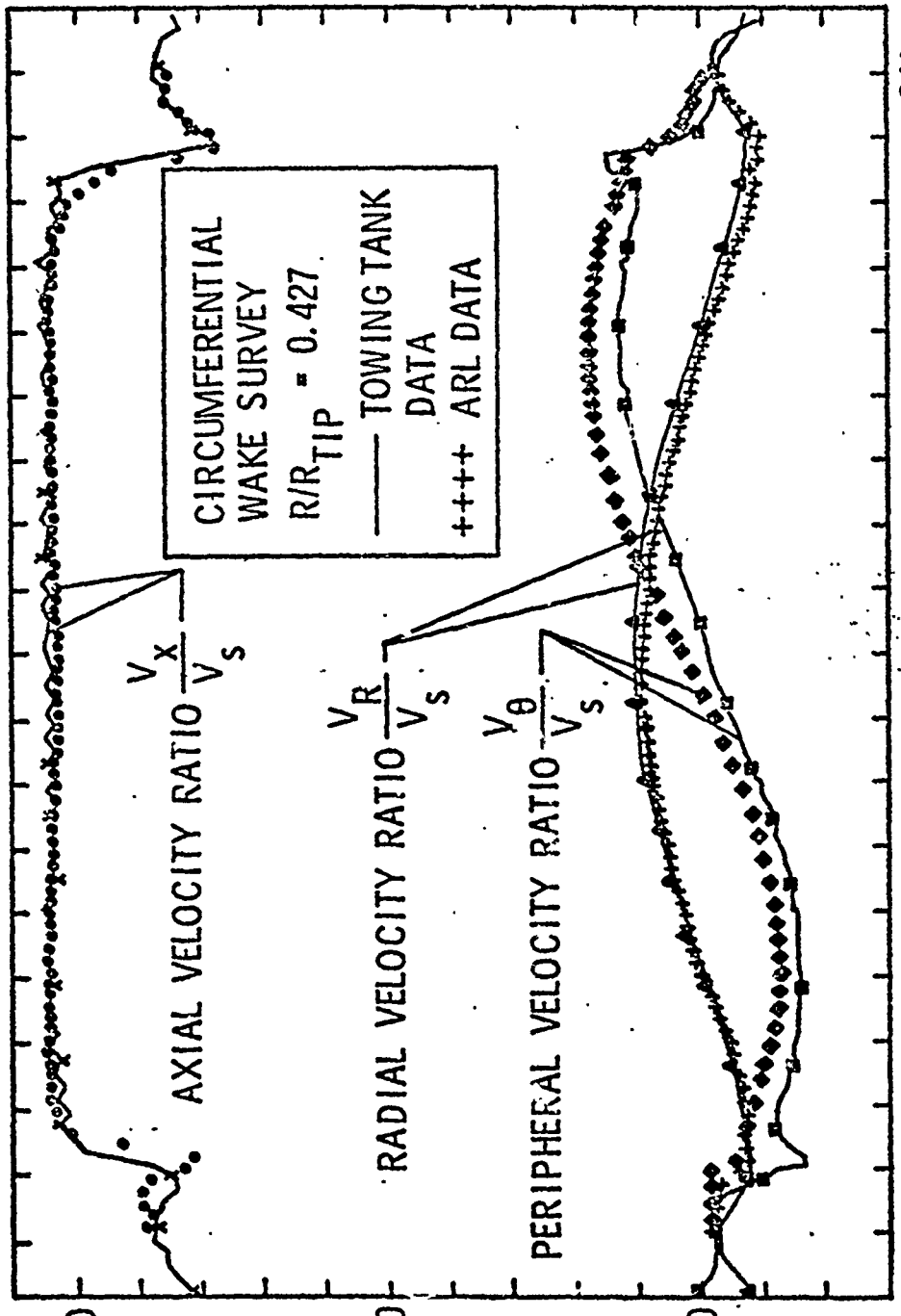

Fig. 16 - TYPICAL SURFACE SHIP CIRCUMFERENTIAL WAKE SURVEY

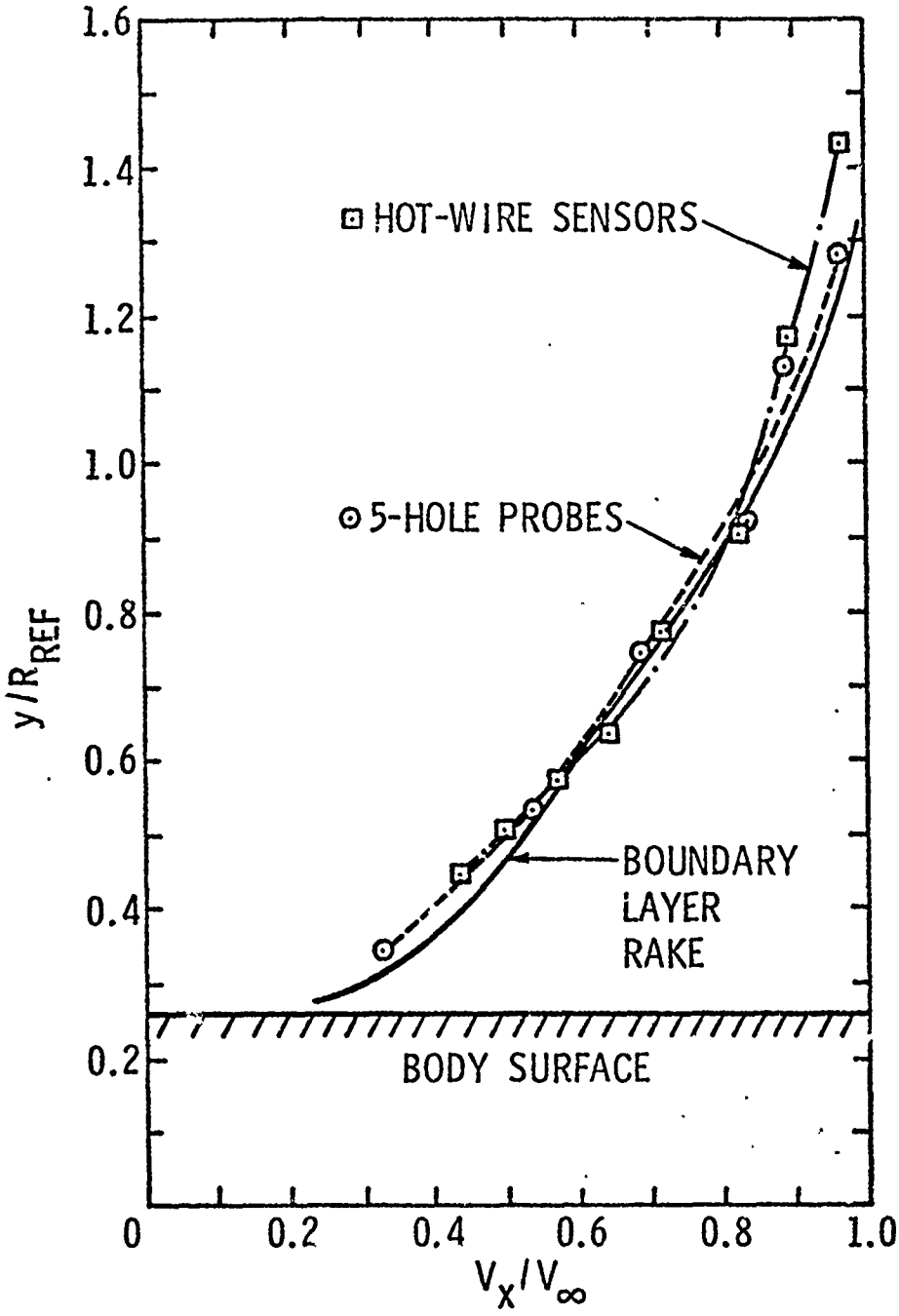

Fig. 17 - COMPARATIVE BOUNDARY LAYER SURVEYS WITH THREE TYPES OF INSTRUMENTATION

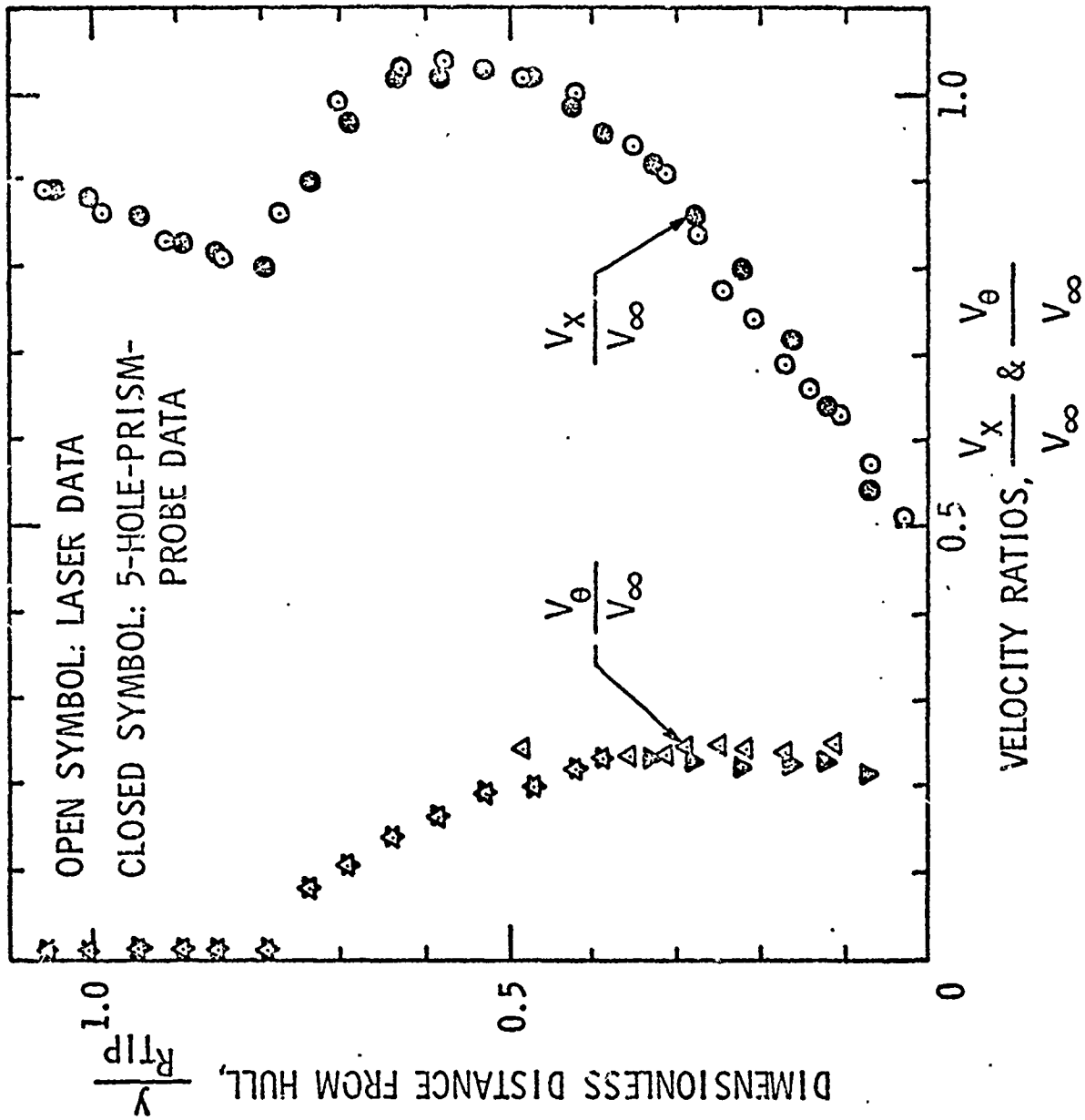

Fig. 18 - COMPARATIVE PROPELLER WAKE SURVEYS

DISTRIBUTION LIST FOR UNCLASSIFIED TM 78-10 by A. L. Treaster and A. M. Yocum
(dated 18 January 1978)

Commander
Naval Sea Systems Command
Department of the Navy
Washington, DC 20360
Attn: Library
Code NSEA-09G32
(Copies 1 and 2)

Naval Sea Systems Command
Attn: J. E. Peirce
Code NSEA-0351
(Copy No. 3)

Naval Sea Systems Command
Attn: A. R. Paladino
Code NSEA-0371
(Copy No. 4)

Naval Sea Systems Command
Attn: H. Claybourne
Code NSEA-0371
(Copy No. 5)

Naval Sea Systems Command
Attn: J. G. Juergens
Code NSEA-037
(Copy No. 6)

Commander
Naval Ship Engineering Center
Department of the Navy
Washington, DC 20360
Attn: W. L. Louis
Code 6136B
(Copy No. 7)

Commanding Officer
Naval Underwater Systems Center
Newport, RI 02840
Attn: Technical Director
Code SB3
(Copy No. 8)

Commanding Officer
Naval Ocean Systems Center
San Diego, CA 92152
Attn: J. W. Hoyt
Code 2501
(Copy No. 9)

Commander
Naval Surface Weapon Center
Silver Spring, MD 20910
Attn: Library
(Copy No. 10)

Commander
David W. Taylor Naval Ship Res. & Dev. Center
Department of the Navy
Bethesda, MD 20084
Attn: W. B. Morgan
Code 154
(Copy No. 11)

David W. Taylor Naval Ship Res. & Dev. Center
Attn: R. Cumming
Code 1544
(Copy No. 12)

David W. Taylor Naval Ship Res. & Dev. Center
Attn: M. Sevik
Code 019
(Copy No. 13)

David W. Taylor Naval Ship Res. & Dev. Center
Attn: T. Brockett
Code 1544
(Copy No. 14)

David W. Taylor Naval Ship Res. & Dev. Center
Annapolis Laboratory
Annapolis, MD 21402
Attn: J. G. Stricker
Code 2721
(Copy No. 15)

Defense Documentation Center
5010 Duke Street
Cameron Station
Alexandria, VA 22314
(Copies 16 - 27)

Von Karman Inst. for Fluid Dynamics
Turbomachinery Laboratory
Rhode-Saint-Genese
BELGIUM
Attn: Library
(Copy No. 28)

DISTRIBUTION LIST FOR UNCLASSIFIED TM 78-10 by A. L. Treaster and A. M. Yocum
(dated 18 January 1978)

Mr. W. Whippen
Allis-Chalmers
Box 712
York, PA 17405
(Copy No. 29)

Dr. G. K. Serovy
Professor
Mechanical Engineering Dept.
Iowa State University
Ames, Iowa 50010
(Copy No. 30)

U. S. Naval Post Graduate School
Monterey, CA 93940
Attn: Library
(Copy No. 31)

Wright Patterson Air Force Base
Dayton, OH 45433
Attn: Dr. William H. Heiser
(Copy No. 32)

Dr. A. J. Acosta
Professor of Mechanical Engineering
Div. of Engr. & Applied Science
California Institute of Technology
Pasadena, CA 91125
(Copy No. 33)

Mr. M. J. Hartmann
NASA Lewis Research Center
21000 Brookpark Road
Cleveland, OH 44135
(Copy No. 34)

SRC Turbomachinery Laboratory
Madingley Road
Cambridge
ENGLAND
Attn: Library
(Copy No. 35)

Hydronautics, Inc.
Pindell School Road
Laurel, MD 20810
Attn: Library
(Copy No. 36)

Mr. A. Mitchell
Admiralty Marine Technology Establishment
Teddington, Middlesex
ENGLAND
(Copy No. 37)

Dr. J. H. Horlock
Vice Chancellor
University of Salford
Salford
ENGLAND
(Copy No. 38)

Netherlands Ship Model Basin
Haagsteeg 2
P. O. Box 28
Wageningen
THE NETHERLANDS
Attn: Dr. P. van Oossanen
(Copy No. 39)

Mr. H. J. Baiter
Forschungsbeauftragter Hydroakustik
8012 Ottobrunn Bei München
Postfach 260
GERMANY
(Copy No. 40)

Dr. R. E. Henderson
The Pennsylvania State University
Applied Research Laboratory
Post Office Box 30
State College, PA 16801
(Copy No. 41)

Mr. A. L. Treaster
The Pennsylvania State University
Applied Research Laboratory
Post Office Box 30
State College, PA 16801
(Copy No. 42)

Mr. A. M. Yocum
The Pennsylvania State University
Applied Research Laboratory
Post Office Box 30
State College, PA 16801
(Copy No. 43)

DISTRIBUTION LIST FOR UNCLASSIFIED TM 78-10 by A. L. Treaster and A. M. Yocum
(dated 18 January 1978)

Garfield Thomas Water Tunnel Library
The Pennsylvania State University
Applied Research Laboratory
Post Office Box 30
State College, PA 16801
(Copy No. 44)